eNeuro

Research Article: New Research | Disorders of the Nervous System

Restrained Dendritic Growth of Adult-born Granule Cells Innervated by Transplanted Fetal GABAergic Interneurons in Mice with Temporal Lobe Epilepsy

Jyoti Gupta[3], Mark Bromwich[3], Jake Radell[3], Muhammad N Arshad[3], Selena Gonzalez[3], Bryan W Luikart[4], Gloster B Aaron[3] and Janice R Naegele[3]

[3]*Department of Biology, Program in Neuroscience and Behavior, Hall-Atwater Laboratory, Wesleyan University, Middletown, CT 06459-0170*

[4]*Department of Molecular and Systems Biology, Geisel School of Medicine, Lebanon, NH 03756*

https://doi.org/10.1523/ENEURO.0110-18.2019

Received: 19 March 2018

Revised: 11 March 2019

Accepted: 15 March 2019

Published: 27 March 2019

J.G. and J.R.N. designed research; J.G., M.B., J.R., M.N.A., S.G., and J.R.N. performed research; J.G. and J.R.N. analyzed data; J.G. and J.R.N. wrote the paper; B.W.L., G.B.A., and J.R.N. contributed unpublished reagents/analytic tools.

Funding: HHS | NIH | National Institute of Neurological Disorders and Stroke (NINDS)
R15NS072879-01A1
;

Funding: HHS | NIH | National Institute of Mental Health (NIMH)
R01MH097949
;

Funding: Citizens United for Research in Epilepsy (CURE)
Challenge Award
;

Funding: Connecticut Regenerative Medicine Fund
13-SCC-WES-01
.

Conflict of Interest: Authors report no conflict of interest.

Submitting author: Jyoti Gupta

This work was supported by NINDS grant R15NS072879-01A1, Connecticut Stem Cell Established Investigator Grant, and a Challenge Award from Citizens United for Research in Epilepsy (J.R.N.) and R01MH097949 (B.L.)

Correspondence should be addressed to Janice R Naegele at jnaegele@wesleyan.edu

Cite as: eNeuro 2019; 10.1523/ENEURO.0110-18.2019

1. Manuscript Title (50 word maximum): Restrained Dendritic Growth of Adult-born Granule Cells Innervated by Transplanted Fetal GABAergic Interneurons in Mice with Temporal Lobe Epilepsy

2. Abbreviated Title (50 character maximum): GABA transplant-induced dendritic growth restraint

3. List all Author Names and Affiliations in order as they would appear in the published article:

Jyoti Gupta[1,3], Mark Bromwich[3], Jake Radell[3], Muhammad N Arshad[3], Selena Gonzalez[3], Bryan W Luikart[4], Gloster B Aaron[3], Janice R Naegele[2,3]

[1] Submitting author

[2] Corresponding author

Author Affiliations:

[3] Department of Biology, Program in Neuroscience and Behavior, Hall-Atwater Laboratory, Wesleyan University, Middletown, CT 06459-0170

[4] Department of Molecular and Systems Biology, Geisel School of Medicine, Lebanon, NH 03756

4. Author Contributions: JG and JRN designed research; JG, MB, JR, MNA, SG, JRN performed research; BL, GBA, JRN contributed reagents/analytic tools; JG analyzed data; JG and JRN wrote the paper. MB and JR contributed equally.

5. Correspondence should be addressed to (include email address): jnaegele@wesleyan.edu

6. Number of Figures: 12

7. Number of Tables: 4

8. Number of Multimedia: 1

9. Number of words for Abstract: 250

10. Number of words for Significance Statement: 148

11. Number of words for Introduction: 864

12. Number of words for Discussion: 1365

13. Acknowledgements: The authors thank Kevin Cobbol, Toria Bobbitt, Meijie Li and Jeff Gilarde for technical assistance, and Meghan Van Zandt, Daniel B Lawrence for helpful discussions about the manuscript. We also thank Nicolas I Woods, Ashley Fine, Elizabeth Paquette for pilot studies of retroviral labeling and neuronal reconstructions. We acknowledge the assistance of Sera Brown and Angela Lentini for help with animal husbandry, and Robert Kabacoff for statistical analyses.

14. Conflict of Interest: Authors report no conflict of interest.

15. Funding sources: This work was supported by NINDS grant R15NS072879-01A1, Connecticut Stem Cell Established Investigator Grant, and a Challenge Award from Citizens United for Research in Epilepsy (J.R.N.) and R01MH097949 (B.L.)

Abstract

The dentate gyrus (DG) is a region of the adult rodent brain that undergoes continuous neurogenesis. Seizures and loss or dysfunction of GABAergic synapses onto adult-born dentate granule cells (GCs) alter their dendritic growth and migration, resulting in dysmorphic and hyperexcitable GCs. Additionally, transplants of fetal GABAergic interneurons in the DG of mice with temporal lobe epilepsy (TLE) result in seizure suppression, but it is unknown whether increasing interneurons with these transplants restores GABAergic innervation to adult-born GCs. Here we address this question by retroviral birth-dating GCs at different times up to 12 weeks after pilocarpine-induced TLE in adult mice. ChR2-EYFP-expressing MGE-derived GABAergic interneurons from E13.5 mouse embryos were transplanted into the DG of the TLE mice and GCs with transplant-derived inhibitory post-synaptic currents were identified by patch-clamp electrophysiology and optogenetic interrogation. Putative synaptic sites between GCs and GABAergic transplants were also confirmed by intracellular biocytin staining, immunohistochemistry, and confocal imaging. 3D reconstructions of dendritic arbors and quantitative morphometric analyses were carried out in >150 adult-born GCs. GABAergic inputs from transplanted interneurons correlated with markedly shorter GC dendrites, compared to GCs that were not innervated by the transplants. Moreover, these effects were confined to distal dendritic branches and a short time window of 6-8 weeks. The effects were independent of seizures as they were also observed in naïve mice with MGE transplants. These findings are consistent with the hypothesis that increased inhibitory currents over a smaller dendritic arbor in adult-born GCs may reduce their excitability and lead to seizure suppression.

Significance statement

Transplants of medial-ganglionic eminence (MGE) GABAergic progenitors into the hippocampus of adult mice with pilocarpine-induced TLE have been shown to increase inhibitory synaptic currents in granule cells (GCs) in the dentate gyrus (DG) and suppress seizures. Here we investigated whether the increased transplant-derived inhibition resulted in structural changes to the dendritic arbors of adult-born GCs that might be responsible for reduced excitability. Our results show that transplant-innervated adult-born GCs form significantly shorter dendrites compared to non-innervated GCs. These changes were restricted to distal dendrites in GCs generated within two-months after transplantation. These findings suggest a structural mechanism for seizure suppression whereby increased GABAergic innervation from transplanted MGE progenitors may restrict the growth of dendritic arbors in adult-born hippocampal granule cells.

Introduction

Hippocampal neural circuit dysfunction is thought to contribute to epileptogenesis and the development of spontaneous seizures in temporal lobe epilepsy (TLE) (Goldberg and Coulter, 2013; Alexander et al., 2016). Mounting evidence suggests that disruptions to the normal pattern of adult neurogenesis in the dentate gyrus (DG) promote the development of hyperexcitability (Parent et al., 1997; Jessberger et al., 2005; Jessberger et al., 2007). Prolonged seizures, defined as status epilepticus (SE) alter granule cell (GC) neurogenesis in the DG of the hippocampus (Parent et al., 1997; Hattiangady et al., 2004; Jessberger et al., 2005; Hattiangady and Shetty, 2010). Following SE, many adult-born GCs migrate to ectopic locations in the hilus or molecular layer of the DG (Scharfman et al., 2000; Scharfman et al., 2003b; Scharfman, 2005; Parent et al., 2006) and form basal dendrites that establish abnormal and hyperexcitable neural circuits (Thind

et al., 2008; Murphy et al., 2011). Studies have shown that number of hilar ectopic adult-born GCs positively correlates with the seizure burden and experimentally ablating GCs born after SE reduces the seizure burden in TLE (Hester and Danzer, 2013; Cho et al., 2015; Hosford et al., 2016; Hosford et al., 2017). Paradoxically, although ablating adult-born GCs in rodents with SE reduced the incidence of seizures, it increased the duration of residual seizures, possibly due to eliminating both normotopic and ectopic adult-born GCs (Hosford et al., 2016 (Yu and Krook-Magnuson, 2017).

The patterns of excitatory and inhibitory connections to both the adult-born and developmentally-born GCs are also altered in TLE (Du et al., 2017). Several factors contribute to this phenomenon, including mossy fiber sprouting (Okazaki et al., 1995; Buckmaster et al., 2002; Scharfman et al., 2003a; Buckmaster, 2012), dendritic hypertrophy (Patel et al., 2004; Arisi and Garcia-Cairasco, 2007; Walter et al., 2007; Nishimura et al., 2008), and dendritic spine loss (Jiang et al., 1998). Prolonged SE can also trigger excitotoxic cell death of hippocampal GABAergic interneurons and lead to compensatory sprouting of surviving interneurons (Zhang et al., 2009; Long et al., 2011; Peng et al., 2013; Buckmaster et al., 2017). Exactly how each of these changes contributes to hyperexcitability is not fully understood (Beck et al., 1996; Bausch and McNamara, 2000; Cossart et al., 2001; Althaus et al., 2015). However, these and other experimental findings support the hypothesis that SE triggers structural and functional modifications to neural circuits in the dentate gyrus that promote hyperexcitability and the development of recurrent spontaneous seizures (SRS) in TLE. Considerable research is now focusing on understanding the cellular and molecular mechanisms for these structural and functional changes in TLE (Pun et al., 2012; LaSarge et al., 2015; LaSarge et al., 2016; Nishimura et al., 2017; Santos et al., 2017). Converging evidence supports the hypothesis that

abnormal cellular growth mechanisms and altered gene expression lead to progressive changes that are sufficient to cause recurrent seizures and epilepsy (Parent et al., 1997; Parent et al., 2006; Walter et al., 2007).

Prior work established that transplanting fetal rodent GABAergic interneuron progenitors harvested from the medial ganglionic eminence (MGE) or purified GABAergic interneurons derived from human embryonic stem cells is effective for suppressing seizures in developmental and chemoconvulsant models of epilepsy (Baraban et al., 2009; Zipancic et al., 2010; Hunt et al., 2013; Cunningham et al., 2014; Henderson et al., 2014; Lee et al., 2014; Shetty and Upadhya, 2016). Some evidence suggests that MGE transplants also reduce mossy fiber sprouting (Henderson et al., 2014; but see Hunt et al. 2013). After transplantation into the hippocampus of mice with TLE, fetal mouse MGE progenitors were linked to increased spontaneous inhibitory postsynaptic currents in hippocampal GCs (Henderson et al., 2014) and increased phasic and tonic inhibition in other populations of host brain neurons (Baraban et al., 2009; Hsieh and Baraban, 2017) via alpha 4 subunit containing $GABA_A$-receptors (Jaiswal et al., 2015). The notion that transplanted neurons integrate into host brain circuits and provide synaptic inhibition is further supported by optogenetic experiments showing that stimulation of transplanted ChR2-expressing GABAergic neurons induced strong post-synaptic inhibitory currents in hippocampal neurons (Henderson et al., 2014; Hsieh and Baraban, 2017). Other mechanisms may also be involved, as MGE progenitor grafts were shown to induce critical period plasticity and rewiring in the spinal cord and cerebral cortex (Park et al., 2002; Lee et al., 2007; Southwell et al., 2010; Chohan and Moore, 2016; Spatazza et al., 2017).

As a further step toward defining the cellular mechanisms responsible for fetal GABAergic interneuron-mediated effects in TLE, we examined whether transplantation of mouse MGE

progenitors into the DG of naïve or TLE mice altered the morphological development of adult born GCs. We found that compared to adult-born GCs that were not innervated by the transplanted cells, the adult-born GCs with fetal transplant innervation exhibited significantly smaller dendritic arbors and shorter distal dendrites. These changes to the dendritic arbors were chiefly within the outer molecular layer of the DG, where adult-born GCs normally receive excitatory inputs from the lateral entorhinal cortex (Woods et al., 2018). The overall growth of dendritic arbors was also reduced in adult-born GCs in naïve, non-epileptic mice that received innervation from transplanted GABAergic interneurons, suggesting a general mechanism whereby inhibitory inputs from transplanted MGE-derived GABAergic interneurons diminish dendritic growth.

Materials and Methods

All materials are listed in Table 1 except for common laboratory reagents that were purchased from Sigma.

Animals

Animal protocols were approved by the Institutional Animal Care and Use Committee (IACUC). As differences in estrous cycle in female mice were reported to affect seizure susceptibility, we performed all studies in male C57BL/6NHsd adult mice (Envigo) to reduce animal use (Muller et al., 2009). The mice were purchased at 4-6 weeks of age and maintained singly in self-ventilating cage racks in the animal facility. They were placed on a 12-hour light/dark cycle and provided with food and water *ad libitum*. The mice were handled daily for 1-2 weeks before seizures were induced. MGE-derived GABAergic progenitors for transplantation were obtained from timed-pregnant C57BL/6NHsd female mice (Envigo) bred adult male

transgenic mice expressing Channelrhodopsin 2 (ChR2)-Enhanced Yellow Fluorescent Protein (EYFP) under the control of the vesicular GABA promoter (VGAT) (VGAT-ChR2-EYFP line 8 (JAX Stock No. 014548, B6.Cg-Tg (Slc32a1-COP4*H134R/EYFP)8Gfng/J) (Zhao et al. 2011), as described below.

Pilocarpine and Drug Administration

The pilocarpine model was used to replicate TLE in 6-8 week-old male mice (Envigo, C57Bl/6N strain, 18-22g), as described previously (Henderson et al., 2014). Seizures were induced in male mice, since females in this mouse strain show significant differences in seizure latency, which could increase variability in patterns of recurrent seizure severity and incidence (Muller et al., 2009). On the day of seizure induction, the male mice were injected with methyl-scopolamine (0.5mg/mL; i.p.; Sigma-Aldrich), followed 30 minutes later by an injection of pilocarpine hydrochloride (280 mg/kg; i.p.; Sigma-Aldrich). One or two supplemental doses of pilocarpine (30-60 mg/kg; i.p.) were administered 30 minutes after the initial injection, if the mouse failed to develop seizures that progressed to SE. Seizures were rated behaviorally, based on a modified Racine scale until the animal reached SE (Shibley and Smith, 2002; Henderson et al., 2014). One hour after continuous SE, seizures were attenuated by injecting midazolam (9.1-11.1 mg/kg; i.p.; Akorn). Ringer's solution (1 ml; i.p.; Henry Schein) was administered as needed, until recovery. A total of 124 mice were induced by pilocarpine. Of these, 77 developed SE (63%), 47 either died during SE or failed to develop SE and were euthanized (37%). Of the 77 SE mice, 44 underwent stereotaxic surgery to inject retrovirus and medial ganglionic eminence (MGE)-derived GABAergic progenitors in the dentate gyrus and 41 of these mice were then used for slice electrophysiology and neuronal reconstructions. A total of 17 C57Bl/6N

male mice (6-8-week-old, 18-22g) did not receive pilocarpine and were used as naïve, non-epileptic controls; 13 underwent stereotaxic surgery to inject retrovirus and MGE-derived GABAergic progenitors in the dentate gyrus of the hippocampus. These mice were subsequently used for slice electrophysiology and neuronal reconstructions. Three naïve (non-epileptic) mice received (MGE)-derived GABAergic progenitor transplants and were used for immunohistochemical analyses of the transplanted cells.

Viral Production and Injection

We labeled adult-born GCs in naïve mice and in mice with pilocarpine-induced TLE by stereotaxic injections a Moloney Murine Leukemia Virus (MMLV) based retroviral vector (Luikart et al., 2011; Luikart et al., 2012) into the subgranular zone of the DG. In mice with SE, the times were selected to coincide with early stages of seizure-induced up-regulation of adult neurogenesis (1 or 2 weeks after induction of SE) or the chronic phase of TLE (6 or 12 weeks post-SE).

The MMLV-based retrovirus was produced by transient transfection of GP2-293 retroviral packaging cell line with a retrovirus containing a plasmid with internal ubiquitin promoter driven mCherry (redRubi) and vesicular stomatitis virus glycoprotein (VSVg). The supernatant containing the viral particles was purified using PEG6000, as described previously (Luikart et al., 2011; Luikart et al., 2012). The retrovirus titer produced in our laboratory was 1-10×10^8 transfection units per microliter (TU/μL).

Twenty-four hours prior to stereotaxic surgery, the mice were given overnight access to running wheels (ENV-044, ENV-044-02; Med Associates Inc.) to activate neurogenesis (Holmes et al., 2004). Thirty minutes before stereotaxic injections of virus, the mice were injected with

Meloxicam (0.03 mL; s.c.; Boehringer Ingelheim). Anesthesia was induced by isoflurane inhalation (Isothesia, Henry Schein) and lidocaine hydrochloride was applied to the skin overlying the midline of the skull for topical anesthesia (2% topical; Hi·Tech Pharmacal). Each mouse received eight stereotaxic injections of retrovirus (0.5 µL per site); the injections were made bilaterally into four sites in each hippocampus at a rate of 0.25 µL/minute with a glass syringe (10 µl, removable needle, Hamilton) equipped with a 30-gauge needle (30 GA, 1", point style 2, 45°, Hamilton), at the following coordinates: AP -1.9 mm, ML ± 1.1, DV -2.5 and -2.3; AP -2.5, ML ± 2.1, DV-2.2 and -1.8. For two injection sites along one needle track, the first injection was made into the more ventral location and the needle remained in place for 2 minutes before a second injection was made into the more dorsal location. The needle was left in place for 5 minutes before being withdrawn and the skin incision was sealed (VetBond tissue adhesive, 3M Corp.). Mice were kept on a heating pad until fully awake and then housed in their home cages.

Transplantation of MGE-derived GABAergic progenitors

MGE-derived GABAergic progenitors were transplanted 2 weeks after SE in mice receiving retrovirus at 1, 6 or 12 weeks after SE, except for one groups of mice that received retrovirus injections 2 weeks after SE; in these mice the GABAergic progenitors were transplanted 6 weeks after SE. Donor cells were harvested from the MGE of E13.5 transgenic mouse embryos derived from adult female breeders (Envigo, C57Bl/6NHsd) bred to VGAT-ChR2-EYFP line 8 (JAX Stock No. 014548, B6.Cg-Tg(Slc32a1-COP4*H134R/EYFP)8Gfng/J) (Zhao et al. 2011). EYFP-positive embryos were identified with specialized goggles (FHS/F-01 headlamp equipped with FHS/EF-2G2 emission filters, Biological Laboratory Equipment

231 Maintenance and Service Ltd.). The MGE on each side of the embryonic brain was isolated by
232 free-hand dissection in cold Hank's balanced salt solution (HBSS, Sigma) without calcium or
233 magnesium, as described previously (Xu et al., 2004; Henderson et al., 2014; Vogt et al., 2015).
234 The tissue was incubated in 0.125% trypsin (Gibco) in HBSS at 37°C for 12 minutes, transferred
235 with fire-polished glass pipettes into trypsin inhibitor (1X, Gibco) for 10 minutes, then
236 mechanically dissociated first with a large bore (10 times) then a small bore, fire-polished glass
237 pipette (10 times). The dissociated cells were centrifuged and suspended in cell transplantation
238 media. Cell counts were performed with a hemocytometer and the cells were then further diluted
239 in cell transplantation media to reach a final concentration of 1×10^5 cells/ml. The
240 transplantation media consisted of L-15 supplemented with fibroblast growth factor (Cell
241 Signaling), epidermal growth factor (Cell Signaling), Caspase Inhibitor (Promega) and B27
242 (Gibco), as described previously (Henderson et al., 2014). The cell suspension was maintained
243 on ice during determination of cell number and then 1 µL (containing~100,000 cells) was slowly
244 injected over the course of 5 minutes into a single injection site into the hilus of the DG, by
245 means of stereotaxic surgery. Bilateral injections were made into each DG (stereotaxic
246 coordinates AP 2.5 mm, ML ±2.1 mm, DV 2.2 and 1.8 mm). The needle was left at the injection
247 site for 5 minutes before being withdrawn. The skin incision was closed, and the mice were
248 allowed to recover on a heated pad, then returned to their cages.
249
250 **Hippocampal slice electrophysiology**
251 After allowing approximately 8 weeks for maturation of adult-born GCs and interneuron
252 transplants, we performed whole-cell patch-clamp recordings of GCs in hippocampal slices, as
253 described previously (Henderson et al., 2014). The mice were anesthetized with a mixture of

ketamine hydrochloride (120 mg/kg; i.p.; Ketaset, Zoetis) and xylazine (10 mg/kg; i.p.; Anased, Lloyd Laboratories), before rapidly removing the brain, and transferring it to oxygenated, ice-cold ACSF (high sucrose ACSF; 27.07 mM $NaHCO_3$, 1.5 mM NaH_2PO_4, 1 mM $CaCl_2$, 3 mM $MgSO_4$, 2.5 mM KCl, 222.14 mM sucrose). Brains were mounted onto the chilled stage of a vibratome (Leica VT1000S) in the horizontal plane, bisected in the sagittal plane, and thick slices (350 µm) were cut from ventral to dorsal. The slices were maintained in oxygenated ACSF (37°C; 125 mM NaCl, 1 mM $CaCl_2$, 3 mM $MgSO_4$, 1.25 mM NaH_2PO_4, 25 mM $NaHCO_3$, 2.5 mM KCl, 25 mM glucose, 3 mM myo-inositol, 2 mM Na-pyruvate, 0.4 mM ascorbic acid) and for electrophysiology, slices were individually transferred into a recording chamber containing oxygenated ACSF (125 mM NaCl, 1.5 mM $CaCl_2$, 1.0 mM $MgSO_4$, 1.25 mM NaH_2PO_4, 25 mM $NaHCO_3$, 3.5 mM KCl, 25 mM glucose, 3 mM myo-inositol, 2 mM Na pyruvate, 0.4 mM ascorbic acid). Electrophysiological recordings were obtained from RV-labeled GCs and unlabeled GCs in voltage-clamp mode at 34°C using a Cesium gluconate intracellular solution (135 mM gluconic acid, 135 mM CsOH, 1 mM EGTA, 8 mM MgCl, 0.1 mM $CaCl_2$, 10 mM HEPES, 2 mM Mg-ATP, 0.3 mM Na-GTP) containing biocytin (11 mM, Sigma), to allow us to recover and stain the electrophysiologically-recorded cells at the end of the experiment. To record inhibitory postsynaptic currents (IPSCs), the cells were voltage clamped at +10 mV. To examine putative synaptic connections between the transplanted MGE-derived interneurons and GCs, we optogenetically activated transplanted ChR2-expressing interneurons using blue light pulses and recorded the responses in dentate gyrus GCs, as described previously (Henderson et al., 2014). The blue light stimulus was triggered using Master 8 stimulator (AMP instruments) and consisted of 5 pulses of blue light (5 msec duration each) with an interstimulus interval of 200 msec (Henderson et al., 2014).

Analysis of electrophysiological recordings

The electrophysiological recordings were analyzed offline using IGOR software. The amplitude of each light-induced IPSC was measured. For each GC, the amplitude of induced IPSCs was determined by taking the average of all the induced IPSCs across a trial. We also determined the IPSC latency to the light stimuli by measuring the delay between onset of the light stimulus and IPSC onset in all adult-born GCs that were confirmed to be mCherry^{+} and thus retrovirally (RV) labeled. To calculate the relationship between the magnitude of the light-induced currents in GCs and the number of MGE transplant-derived synaptic puncta, we correlated the peak amplitude of light-induced currents to the total number of synaptic appositions counted with the "Spots" function in IMARIS software, as described below.

Immunohistochemical staining of thick slices

Following electrophysiological recordings, the slices were fixed overnight in 4% paraformaldehyde (Electron Microscopy Sciences). The slices were then equilibrated in phosphate-buffered saline containing 30% sucrose and frozen in tissue freezing medium (General Data).

To confirm RV-labeling in electrophysiologically-identified GCs within the vicinity of transplants of MGE-derived interneurons, we immunostained all the slices for mCherry, eYFP and biocytin. The slices were thawed and transferred to blocking buffer (5% normal goat serum containing 0.3% Triton-X) for 1 hour at RT. Slices were incubated for 48 hours at RT in primary antibody solution in blocking buffer containing: chicken anti-GFP (1:1000, Aves), rabbit anti-mCherry (1:1000, Invitrogen), and Streptavidin Alexa-647 (1:500, Invitrogen; omitted when

staining slices that did not contain biocytin-filled cells). The slices were then washed for one hour in phosphate buffered saline (KPBS, 0.02M) and transferred into secondary antibody solution containing goat anti-rabbit Alexa 568 (1:1000, Life Technologies) and goat anti-chicken Alexa 488 (1:1000, Life Technologies) for 24 hours, before a final wash for 1 hour. Sections were mounted on Superfrost Plus slides in Prolong Gold with DAPI (Invitrogen) and stored at -20 in the dark.

Phenotypic Characterization of Transplanted Cells

Three additional SE mice with MGE-derived GABAergic progenitor transplants were perfused with 4% paraformaldehyde in 0.1M Phosphate Buffer (pH 7.4) and the brains were equilibrated in ascending sucrose solutions (10, 20, and 30% sucrose in 0.1M Phosphate Buffer, pH 7.4), then frozen in tissue freezing media (General Data). Forty μm thick cryostat sections were collected in 0.1M PBS and immunofluorescent staining was performed to detect transplanted GABAergic interneurons expressing ChR2-EYFP (chicken anti-GFP, GFP 1020, Aves), in combination with one of the following neurochemical markers: parvalbumin (PV; rabbit anti-parvalbumin, 1:100, PV-27, Swant), somatostatin (SOM; rat anti-somatostatin, 1:100, mab354 Millipore), calretinin (CR; rabbit anti-calretinin, 1:100, ab704 Abcam), or neuronal nitric oxide synthase (nNOS; rabbit anti-nNOS, 1:1000, AB5380, Millipore). Incubations were performed on free-floating sections at 4°C for 48 hours with agitation. Sections were washed in PBS and secondary antibodies were applied as follows: AlexaFluor 568 and AlexaFluor 488. Nuclei were labeled with NeuroTrace Nissl 647 (1:300, Life Technologies) and sections were mounted onto glass slides in Prolong with DAPI (Life Technologies). We quantified the neurochemical phenotypes of all single and double-labeled cells contained in the hippocampus in

323 a total of 20-24 sections/mouse. For each mouse, six sections spaced 400 microns apart were
324 immunostained for EYFP and one of the four neurochemical markers. Using optical slices
325 obtained from confocal microscopic images of the hippocampal sections, we quantified the total
326 number of individual, transplanted $EYFP^+$ interneurons in each hippocampus and the number
327 that co-expressed an additional neurochemical marker.
328
329 **Confocal Imaging**
330 For imaging biocytin-filled GCs and the neurochemical phenotypes of transplanted cells,
331 we collected optical slices through the entire thickness of 350 micron-thick fixed and stained
332 hippocampal slices that had been used for electrophysiological studies. Confocal microscopy
333 (Zeiss LSM 510 or a Leica SP8) was performed at 0.5 µm steps using a 25x objective (Zeiss
334 Plan-Neofluar 25x, N.A. 0.8, water immersion objective) and a 63x objective (Zeiss C-
335 Apochromat 63x objective, N.A. 1.2, water immersion). For Sholl analyses, RV-labeled GCs
336 were imaged at lower magnifications to record their positions and capture the entire dendritic
337 arbors (Zeiss Plan-Apochromat 10x, N.A. 0.45 and Zeiss Plan-Neofluar 25x, N.A. 0.8, water
338 immersion objectives; z-stacks with a step size of 1 µm and frame size, 1024×1024 pixels). For
339 detection and quantification of putative synaptic contacts formed by the transplanted GABAergic
340 interneurons onto RV-labeled GCs, we imaged each RV-labeled neuron at high magnification
341 (C-Apochromat 63x objective, N.A. 1.2, water immersion). These high-resolution images were
342 obtained as z-stacks with a step size of 0.3 µm and resolution of 2048 by 2048 pixels. All
343 confocal images were stored on local hard drive (Backup Plus Desktop Drive, Seagate
344 Technology) and archived in long-term cloud storage (RStore).
345

346 **3D Reconstructions and Dendritic Arbor Morphometric Analyses**

347 To analyze dendritic morphology in RV-labeled adult-born GCs, confocal z-stacks of cells
348 were imported into IMARIS neuron reconstruction software (8.4.0, Bitplane). The dendrites
349 were traced using the filament tracer tool. Morphometric analyses of the reconstructed dendritic
350 arbors were performed to quantify the following cell properties: total dendritic length, number of
351 different order branches, length of different branches and number of branch points. For dendritic
352 branch lengths and total dendritic lengths, the distance from the center of the soma to the
353 beginning of the primary dendrite was excluded. To determine dendritic complexity, three-
354 dimensional Sholl analyses were performed from the center of GC somas in IMARIS, identifying
355 dendritic branch intersections at 10 μm intervals.

356 Because electron microscopy has not been used to confirm that the axonal swellings formed
357 by the transplanted neurons onto the GCs in the host brains are bona fide inhibitory GABAergic
358 synapses, we refer to these morphological swellings as "putative synapses" throughout the
359 manuscript. To quantify putative transplant-derived synapses onto RV-labeled GCs, the "Spots"
360 function in IMARIS was used to identify green fluorescent boutons within 0.5 μm of the cell that
361 had a diameter of about 0.75 μm or larger. Each putative synapse was checked manually to
362 eliminate false signals. It seems probable that a many of these "putative synapses" are sites of
363 neurotransmitter release, as it was previously demonstrated by optogenetic studies that light-
364 induced depolarization of the transplanted cells induced strong IPSCs in nearby GCs with short
365 latencies (Henderson et al., 2014). Additionally, ~60% of these axonal swellings were previously
366 found to be closely associated with postsynaptic clusters of gephyrin, an inhibitory synapse-
367 specific postsynaptic density protein (Henderson et al., 2014).

We further classified the RV-labeled adult-born GCs based on patterns of innervation; the adult-born GCs that had fewer than 15 transplant-derived boutons on the entire cell were classified as "non-innervated" by the transplanted cells whereas GCs with greater than 15 transplant-derived putative synapses were classified as "innervated". The Sholl analyses were performed on adult-born GCs that were RV-labeled after SE as follows: RV1 week: 42 GCs (29 non-innervated and 13 innervated; RV2 weeks: 27 GCs (16 non-innervated and 11 innervated); RV6 weeks: 30 GCs (20 non-innervated and 10 innervated); 12 weeks: 27 GCs (10 non-innervated and 17 innervated).

Statistical analyses

All statistical analyses were performed in SAS, version 9.4 (SAS Institute). Sholl intersection data was analyzed using a mixed-effects model with an auto-regressive variance structure and multi-level nesting along with the use of MULTTEST procedure to correct for false discovery rates, due to multiple t-tests (Wilson et al., 2017). Analyses of the length and numbers of different order branches were also performed using a mixed model. Comparisons of the means of the total dendritic lengths across different groups were done with ANOVA. Data are presented as the mean +/- SEM.

Results

What is the spatio-temporal pattern of adult-neurogenesis in the hippocampus at different times after SE?

Given that adult-born GCs display morphological and functional abnormalities and are believed to contribute to hyperexcitability in the pilocarpine model, we first characterized adult-

born GCs generated in naïve and epileptic mice at different times after SE by RV-labeling and confocal microscopy. To this end, we made RV injections into the subgranular zone of the DG in naïve and epileptic mice at 1, 2, 6, or 12 weeks after inducing SE and allowed 1-2 months for the adult-born neurons to reach maturity before analyzing patterns of neurogenesis (Figure 1A). Retroviral expression of mCherry completely filled the soma, dendrites and frequently the axons of adult born GCs (Figure 1B). In naïve mice, we observed strong labeling of GCs throughout the granule cell layer (GCL) of the DG (Figure 1C). In epileptic mice, robust labeling of adult-born GCs was observed in the GCL and occasionally in the hilus or subgranular zones of the DG, following retroviral injections at 1, 2 or 6 weeks after SE (Figure 1 D-F). In agreement with prior studies, chronically epileptic mice injected with retrovirus 12 weeks after SE exhibited sparser labeling with more frequent clumps of adult-born GCs (Figure 1G).

[Insert Figure 1 about here].

Do adult-born GCs receive functional inhibition from developing MGE transplants?

Given that MGE-derived GABAergic interneuron progenitors take approximately 4 weeks to mature after transplantation (Southwell et al., 2010), we allowed ~8 weeks for both the transplanted cells and the retrovirally-labelled GCs to mature. The degree of inhibitory synapse formation from the transplants onto adult-born GCs was assessed first by combining optogenetic stimulation with patch-clamp recordings in live hippocampal slices and second, by immunostaining the fixed slices and performing high-resolution confocal imaging.

We first measured the extent of light induced inhibitory currents in GCs, by recording from RV-labeled, adult-born GCs by whole-cell patch-clamp recordings, while optogenetically activating slices containing ChR2-expressing interneuron transplants (Figure 1A timeline). A

representative slice showing transplanted GABAergic interneurons in the hilus and RV-labeled adult-born GCs in the GCL, is shown in Figure 2A. An example of a RV-labeled GC born 1 week after SE that was filled with biocytin and further studied by electrophysiology is shown (insets, magnified views, Figure 2B-D). This neuron received putative transplant-derived synapses onto the dendritic shafts and spines (Figure 2E, arrows) (Chiu et al., 2013). Optogenetic stimulation of transplant-derived interneurons induced strong inhibitory post-synaptic currents (IPSCs) in this adult-born GC (Figure 2G). A complete reconstruction of the dendritic arbor revealed 74 transplant-derived, putative synaptic contacts (Figure 2F). We carried out additional electrophysiological studies in 23 hippocampal slices from 6 mice with RV-labeling at 1-week post-SE and transplants at 2 weeks post-SE. We successfully recorded from 23 mature GCs in these slices and 10 showed IPSCs in response to optogenetic stimulation. Six of the GCs in this subset were also retrovirally labeled. Dendritic branching patterns of all six GCs were reconstructed in IMARIS and we found an average of ~180 putative synapses from the transplanted interneurons onto these GCs and a mean light-induced IPSC amplitude of 63.79 ± 28.42 pA. These results, summarized in Table 1, establish that GCs born 1-week post-SE are heavily innervated by MGE transplants made a week later and that activating the putative synaptic inputs onto these cells induces powerful postsynaptic inhibition.

[Insert Table 1 about here]

[Insert Figure 2 about here].

What functional subtypes of interneurons are present in the transplants?

To further characterize the transplanted GABAergic interneurons that could be responsible for driving the observed postsynaptic inhibitory currents in adult-born GCs, we evaluated the

437 neurochemical subtypes of interneurons within the transplants. We selected molecular markers
438 with little to no overlap in different classes of MGE-derived GABAergic interneurons and show
439 typical immune-staining patterns in Figure 2-1. Approximately 37% of the grafted neurons co-
440 expressed VGAT and PV (207 PV^+/554 $EYFP^+$ cells) and 34% co-expressed VGAT and SOM
441 (232 SOM^+/685 $EYFP^+$ cells). A smaller percentage of about 12% co-expressed VGAT and
442 nNos (73 $nNos^+$/588 $EYFP^+$ cells), and about 8% co-expressed calretinin (52 CR^+/651 $EYFP^+$
443 cells). While the immunohistochemical data show that ~ 71% of the transplanted GABAergic
444 interneurons were either PV- or SOM-positive, any or all of these interneuron subtypes were
445 associated in close proximity with the adult-born GCs.
446 [Insert Figure 2-1 about here]
447
448 **Do MGE transplants innervate GCs born at asynchronous stages of development?**
449 To determine whether transplanted GABAergic interneurons can innervate adult-born GCs
450 that at different stages of maturity, we made retroviral injections at 2 weeks post-SE and
451 transplants at 6 weeks post-SE, then recorded from GCs in these mice 4-8 weeks later. In 8/15
452 cells with strong IPSCs in response to optogenetic stimulation (Figure 3A-A''), *post-hoc* staining
453 confirmed RV-labeling in 2/8 (Mean IPSC amplitudes: 83.8 and 127.4 pA, respectively). These
454 results suggest that optogenetic stimulation of the transplanted cells induced strong inhibition in
455 many of the adult-born GCs (Figure 3A-C).
456
457 **Do later-born GCs receive functional inhibition after MGE transplants have matured?**
458 An additional 13 GCs were recorded from mice with retroviral injections at 6 weeks post-
459 SE and transplants at 2 weeks post-SE (Figure 3B-B"); 8 were confirmed to have RV-labeling

and 5/8 showed light-induced IPSCs (Mean IPSC amplitude 175.8 ± 51.4 pA). To test whether GCs born long after transplants were made would show strong transplant-derived synaptic inhibition, we characterized adult-born GCs in mice that received transplants at 2 weeks post-SE and retroviral injections at 12 weeks post-SE. Remarkably, we found light-induced inhibitory currents in 4 of these RV-labeled GCs (Figure 3C-C'') (185.17 ± 89.27 pA). We were further able to confirm RV-labeling *post-hoc* in one of these cells. As a whole, these findings show that the transplanted GABAergic interneurons are capable of providing functional inhibition onto GCs born several months after development of TLE. In the adult-born GCs that did not show light induced currents (Figure 3D, E), confocal microscopy showed that the cells generally had less than 15 transplant-derived synaptic boutons onto their somas or dendrites. In total, we recorded from 55 GCs in mice with retroviral birth-dating at 1, 2, 6, or 12 weeks after SE. Of the 55 GCs with strong light-induced inhibitory currents, we confirmed retroviral mcherry expression in 14/55 by *post-hoc* immunostaining. Twelve of the 14 retrovirally labeled GCs that were optogenetically-responsive showed a delay of 3 msec or less (mean 1.6 msec, range 1-3 msec) between the beginning of blue light stimulus and IPSC onset, indicating a monosynaptic origin of the optogenetically-induced inhibitory currents onto them. Together, these findings indicate that MGE-derived interneurons continue to innervate and form functional inhibitory connections with adult-born GCs over a relatively long period, in excess of 10 weeks after transplantation.

[Insert Figure 3 about here].

What is the relationship between the number of synaptic inputs from the transplants and light-induced IPSCs?

Having established that transplanted GABAergic interneurons induce hyperpolarizing currents in GCs born at different times after the development of TLE and transplantation, we next asked whether the number of putative synaptic inputs correlated with the strength of the post-synaptic inhibition, which would further strengthen the evidence that the MGE cells formed functional inhibitory synapses onto adult-born GCs. To address this question, we completed high-resolution reconstructions of 24 GCs from 13 mice that were optogenetically stimulated during electrophysiological recordings. As shown in Figure 3, the number of morphologically-identified putative synaptic boutons onto individual GCs ranged from 14 to 1,103 putative synapses/cell. Moreover, the number of these inputs was highly correlated with the peak amplitudes of optogenetically-induced IPSCs onto each cell (Figure 3F; $R^2 = 0.838$). Remarkably, the largest number of transplant-derived synaptic boutons (1,103) was onto a GC born 10 weeks after the GABAergic interneurons were transplanted in a TLE mouse (12 weeks after SE) (Figure 3C). These findings in chronically epileptic mice indicate that the strength (amplitude) of the light-induced inhibitory synaptic currents in adult-born GCs is strongly related to the density of innervation from transplanted interneurons and that long after transplantation, MGE-derived GABAergic interneurons retain a robust capacity for forming putative inhibitory synapses with new adult-born GCs.

Does functional innervation of adult-born GCs require epilepsy-induced circuit reorganization in host brain?

Many studies have shown that pilocarpine-induced SE results in selective loss of SOM^+ interneurons in the hippocampus and sprouting of subsets of interneurons, as well as other host brain changes (Peng et al., 2013). To determine whether changes in the host brain in TLE are

506 required for the transplanted cells to form synaptic inputs onto adult-born neurons, we studied
507 the innervation of adult-born GCs in naïve, non-epileptic mice by retrovirally labeling adult-born
508 GCs in 6-8-week-old naïve mice and then a week later, we transplanted fetal GABAergic
509 interneuron progenitors into the DG. After allowing 8 weeks for maturation of the RV-labeled
510 GCs and transplanted GABAergic interneurons, we made patch-clamp recordings from the
511 labeled GCs, while activating the slices with blue light. Of 39 GCs recorded in slices from 11
512 naive mice with transplants, the majority showed robust light-induced responses (24/39 cells,
513 Mean IPSC amplitude: 76.15 ± 20.51 pA). One representative example of an RV-labeled, adult-
514 born GC from a naïve mouse is shown in Figure 4 (A-C). This GC showed strong light-induced
515 IPSCs (Figure 4D) and had extensive transplant-derived putative synapses onto its soma and
516 dendrites (Figure 4F). Based on our Sholl analyses, this GC had a typical branching profile
517 (Figure 4E). In just under half (42%) of the 31/39 adult-born GCs with confirmed RV-labeling in
518 naïve mice, we were able to demonstrate post-synaptic inhibition by optogenetically stimulating
519 the transplants (13/31 RV-labeled GCs). The remaining 18 RV-labeled GCs were non-innervated
520 and served as an internal control group (also see Figure 6). Taken together, these results
521 demonstrate that MGE-derived GABAergic progenitors transplanted into the adult DG robustly
522 innervate adult-born GCs in both epileptic and naïve, non-epileptic adult mice.
523 [Insert Figure 4 about here]
524

525 **Does innervation by MGE transplants alter the dendritic morphology of adult-born GCs?**
526 As changes in dendritic morphology are well-documented in hippocampal GCs in TLE, our
527 central question was whether the increased inhibition from the transplanted GABAergic
528 interneurons altered the dendritic growth of adult-born GCs. To address this question, we

compared dendritic morphologies in innervated vs. non-innervated adult-born GCs, using high-resolution 3D reconstructions and Sholl analyses of 157 RV-labeled adult-born GCs; including 126 GCs from SE mice and 31 GCs from naïve mice. An example of a GC born at 6 weeks post-SE and innervated by a transplant made at 2 weeks post-SE is shown in Figure 5. The transplant contained a large VGAT-EYFP^{+} interneuron in the vicinity of this GC (Figure 5B, white arrow), shown at higher magnification in Figure C. Excitation of the ChR2-expressing axons in this slice evoked IPSCs in host brain GCs (Figure 5D). The Sholl analysis of the dendritic arbor of this GC indicated a relatively normal pattern of dendritic branching (Figure 5E) and the corresponding 3D morphological reconstruction revealed a high density of transplant-derived putative synapses onto this cell's dendritic arbor (Figure 5F).

[Insert Figure 5 about here].

To determine whether putative synaptic innervation from the transplanted interneurons induced structural changes to the dendritic arbors of adult-born GCs, we examined the total dendritic lengths. Strikingly, the sizes of the dendritic arbors in GCs with heavy input from the transplanted GABAergic interneurons were significantly smaller, compared to non-innervated GCs in the same animals (Figure 6B; total dendritic lengths were on average, 1700.0 ± 92.0 µm in the population of innervated GCs vs. an average of 2055.6 ± 116.4 µm in the sample of non-innervated GCs, *p* value 0.0235). Moreover, a significant effect of transplant-derived innervation was found for GCs born 1, 2, or 6 weeks after SE. When these populations of adult-born neurons were innervated by the transplants, they developed significantly shorter dendrites compared to non-innervated adult-born GCs generated at the same time. Although the retrovirally-labeled GCs born 12 weeks after SE were also heavily innervated by the transplants and showed a similar trend of having shorter dendrites compared to non-innervated GCs, overall the

552 differences in dendritic arbor size were not statistically significant (1917.0 ± 147 µm vs. 2143.3
553 ± 167.3 µm, *p* value 0.3211). The results of the statistical tests of significance for all Sholl data
554 are shown in Table 3.
555
556 Overall, the total dendritic lengths for the innervated vs. non-innervated GCs in different
557 groups and the number of GCs that were analyzed for each group were as follows: in naive mice
558 the total dendritic branches were 1700.0 ± 92.0 µm (n= 13 transplant-innervated GCs) vs. 2055.6
559 ± 116.4µm (n=18 non-innervated GCs) (*p* value 0.0235). In epileptic mice with RV labeling at 1-
560 week post-SE, the total dendritic branch lengths of the transplant innervated vs. non-innervated
561 adult-born GCs were 1690.1 ± 101.5 µm (n=13 transplant innervated GCs) vs. 2039.9 ± 84.0 µm
562 (n=29 non-innervated GCs) (*p* value 0.0129). In epileptic mice with RV labeling at 2 weeks post-
563 SE, the total dendritic lengths of the transplant innervated vs. non-innervated adult-born GCs
564 were 1577.7 ± 140.5 µm (n=11 transplant-innervated GCs) vs. 2161.6 ± 93.0 µm (n=16 non-
565 innervated GCs) (*p* value 0.0027). In epileptic mice with RV-labeling at 6 weeks post-SE, the
566 total dendritic lengths of the transplant innervated vs. non-innervated adult-born GCs were
567 1825.3 ± 120.2 µm (n=10 transplant innervated GCs) vs. 2390.0 ± 70.8 µm (n=20 non-
568 innervated GCs) (*p* value 0.0010). In epileptic mice with RV labeling at 12-weeks post-SE, the
569 total dendritic lengths of the transplant innervated vs. non-innervated adult-born GCs were
570 1917.0 ± 147 µm (n=17 transplant innervated GCs) vs. 2143.3 ± 167.3 µm (n=10 non-innervated
571 GCs) (*p* value 0.3211).
572 Given that the total dendritic lengths of adult-born GCs were significantly smaller when
573 they were innervated by the MGE transplants, we next compared differences in proximal vs.
574 distal dendrite lengths (Figure 6C-H). The GCs from naïve mice that received input from the

MGE transplants showed reductions in the lengths of both proximal and distal dendrites, compared with non-innervated GCs (Radii 50-70 µm and radii 180-240 µm, *p* value <0.05). However, in epileptic mice, dendritic growth was significantly more stunted distally in GCs that were innervated by the transplants (Figure 6D; Radii 170-270 µm, *p* value < 0.01) whereas proximally, dendritic growth was unaffected. The most significant differences were found in 3rd through 7th order branches in GCs innervated by the transplants. For example, the average length of 3rd order branches was 64.4 ± 6.8 µm in innervated GCs. vs. 78.7 ± 4.4 µm in non-innervated GCs (*p* value 0.0390); the average length of 5th order branches in transplant-innervated GCs was 72.2 ± 8.0 µm vs. 108.9 ± 5.1 µm in non-innervated GCs (*p* value 0.0390); the average length of 6th order branches was 34.8 ± 8.6 µm in innervated GCs, vs. 71.3 ± 5.5 µm in non-innervated GCs (*p*<0.0001), and the average length of 7th order branches was 7.5 ± 6.1 µm in innervated GCs vs. 22.0 ± 3.9 µm in non-innervated GCs (*p* value 0.0197). We also found that adult-born GCs generated shortly after induction of SE showed the greatest effects; for example, GCs born 1 week after SE had significantly shorter 3rd, 4th, and 6th order branches (3rd order branches: innervated 47.6 ± 13.6 µm vs. non-innervated 78.9 ± 7.6 µm; *p* value 0.0271); 4th order branches: innervated 73.1 ± 10.7 µm vs. non-innervated 95.6 ± 6.0 µm; *p* value 0.0437); 6th order branches: innervated 34.6 ± 15.4 µm vs. non-innervated 66.7 ± 8.6 µm; *p* value 0.0438). In contrast, GCs generated at 2 weeks post-SE only showed significantly shorter 5th order branches (82.5 ± 16.0 µm vs. 117.6 ± 10.2 µm; *p* value 0.0385), and similarly, GCs generated 6 weeks after SE only showed significantly shorter 5th order (50.3 ± 17.3 µm vs. 108.1 ± 10.0 µm, *p* value 0.0024) and 6th order branches (24.1 ± 20.5 µm vs. 80.6 ± 11.8 µm; *p* value 0.0102).

We further compared branching patterns based on Sholl Analyses for the entire populations of innervated vs. non-innervated GCs born 1, 2, 6, and 12 weeks post-SE (Figure

598 6E-F and Table 2). In all of these groups, except for the GCs born 12 weeks after SE, we found
599 that input from the MGE transplants was linked to a significant reduction in the size of the
600 dendritic arbors, with more restricted growth of the distal dendritic branches. While the GCs
601 generated 12 weeks after SE did not show statistically significant differences in branching, they
602 did show a similar trend toward shorter distal dendritic branches (Figure 6E-F; Table 2 Dendritic
603 Length Data).

604 A larger sample of representative RV-labeled adult-born GCs are shown in extended data
605 figures 6-1 through 6-5. While none of the GCs born in naïve mice were dysmorphic, GCs in
606 epileptic mice exhibited highly abnormal arbors with hilar basal dendrites. Taken together, these
607 results indicate that in epileptic and naïve mice, adult-born GCs with putative synapses formed
608 by the MGE transplants had significantly shorter dendritic arbors.

609 [Insert Figure 6 about here]

610 [Insert Figure 6-1 to 6-5 about here].

611
612 **Discussion**
613
614 We have used a retroviral approach to label adult-born GCs at successively different
615 times in naïve or epileptic mice in combination with transplantation of MGE progenitors from
616 E13.5 ChR2-EYFP^{+} mouse embryos either before or after RV-labeling of adult-born GCs. We
617 allowed for maturation of the transplants and adult-born GCs, then tested for functional
618 integration of the transplants by optogenetically stimulating the transplanted cells, while patch-
619 clamping nearby RV-labeled GCs in hippocampal slices. The GCs were concurrently stained
620 with biocytin during recordings, and after fixing the slices, 3D reconstructions and morphometric
621 analyses were carried out.

The major new findings of this study are that fetal ChR2-expressing fetal mouse GABAergic progenitor transplants in the hippocampus of naïve or epileptic adult mice innervate dentate GCs born weeks or even months after the time of transplantation. Optogenetic stimulation of the transplants induced strong inhibitory postsynaptic currents in adult-born GCs, and the magnitude of these currents correlated with the number of transplant-derived (putative) GABAergic synapses on these adult-born GCs. Additionally in either naïve, non-epileptic mice or epileptic mice, adult-born GCs receiving dense innervation from the transplanted GABAergic interneurons had significantly more compact dendritic arbors, due to reduced growth of distal dendrites.

Remarkably, GCs born during the chronic phase of epilepsy as late as 12 weeks post-SE were heavily innervated by the interneuron transplants and the magnitudes of optogenetically induced postsynaptic inhibitory currents were as large as those observed in populations of adult-born GCs generated shortly after transplantation. However, later born GCs showed a more modest trend toward reduced dendritic growth which was not significantly different from non-innervated GCs, suggesting that transplant-induced effects on adult-born GCs and their dendritic growth may wane over time. It was previously shown that astrogliosis increases in the DG during the chronic phase of TLE, leading to compromised GABAergic inhibition, which could reduce efficacy of the both endogenous and transplanted GABAergic interneurons (Eid et al., 2004; Dengler et al., 2017). Indeed, a previous study examining MGE transplants in mice with TLE, showed that seizure suppression did not endure during the later phases of TLE (Henderson et al., 2014). However, further work is needed to determine whether shorter distal branches in adult-born GCs leads to functional changes that reduce either the connectivity or excitability of dentate GCs.

Relationship to prior studies of GC structural changes in epilepsy

The present study examined structural changes in the dendrites of normotopic adult-born GCs in naïve and SE mice following transplantation and integration of GABAergic progenitors harvested from the fetal mouse MGE. We confined our analyses to normotopic GCs, in order to increase our sample sizes. It would be important in future studies, however, to investigate whether inputs from transplanted fetal GABAergic cells also restrict the growth of dendrites formed by ectopic GCs born in the epileptic brain, as the ectopic adult-born GCs in particular, are thought to contribute to epileptogenesis and hyperexcitability.

Several studies in rodent models of TLE have compared dendritic arbor complexity in normotopic vs. hilar ectopic GCs and reported greater distal GC dendrite branching (Sholl intersections) in epileptic compared to naïve rats (Cameron et al., 2011). Similarly, in tissue from human patients with TLE or extra-hippocampal lesions, GCs were found to have increased dendritic lengths in the inner molecular layer of the dentate gyrus (von Campe et al., 1997). Our findings suggest that transplant-derived input onto GCs reduces both normal dendritic growth and epilepsy-induced dendritic overgrowth.

Role of GABA and downstream signaling pathways in structural changes in adult-born GCs

The observed changes in dendrite growth could be mediated by the spontaneous or synaptic release of GABA from the transplanted interneurons. Adult-born GCs receive their first inputs from GABAergic interneurons (Ge et al., 2006). $GABA_A$ receptor antagonists have revealed tonic GABA currents in developing GCs as early as 3 days after birth and GABA-

668 mediated synaptic currents as early as 7 days after cell birth (Ge et al., 2006). In contrast, the first
669 glutamatergic currents occur about 14 days after GC birth (Ge et al., 2006). Newborn GCs
670 express high levels of Na^{+}-K^{+}-$2Cl^{-}$ transporter NKCC1 and thus, have a high intracellular
671 chloride concentration, which causes GABA to be depolarizing, before a developmental switch
672 to a hyperpolarizing effect of GABA (Ben-Ari et al., 2012). The depolarizing effects of GABA
673 are seen for at least 2 weeks after GC's are born in the rodent (Ge et al., 2006). The initial
674 GABA-mediated depolarization appears to be important for regulating dendritic growth, as
675 knocking down NKCC1 reduced dendritic length and branching up to 14 days after cell birth (Ge
676 et al., 2006).

677 Growth-modulating effects of synaptic or extra synaptic GABA could be mediated by a
678 number of different intracellular signaling pathways. For example, a major mechanism for
679 GABA-mediated modulation of intracellular pathways is through activation of voltage-gated
680 calcium channels that are activated by GABA-mediated depolarization, resulting in calcium
681 influx (Schmidt-Hieber et al., 2004). Consistent with this, application of exogenous GABA to
682 immature cerebellar granule neurons, increased calcium influxes and increased dendritic
683 complexity whereas antagonists of voltage-gated calcium channels inhibiting
684 calcium/calmodulin-dependent protein kinase CaMKII inhibitors reduced dendritic growth
685 (Redmond et al., 2002; Borodinsky et al., 2003). The effects of GABA and calcium influxes on
686 dendrite growth are likely to be mediated through molecules such as CaMKII and CaMKIV, or
687 downstream signaling proteins, such as mitogen-activated protein kinases (MAPK) and protein
688 kinase A (PKA) (Ghosh and Greenberg, 1995) as inhibition of CaMKIV has been linked to
689 reduced dendritic growth, while increased CaMKIV activation has been shown to increase
690 dendritic growth (Redmond et al., 2002).

691 Considering the importance of voltage-gated calcium influxes in GC maturation, it will be
692 important to determine whether innervation of adult-born GCs by fetal GABAergic interneurons
693 alters key intracellular calcium-dependent signaling pathways. One downstream effector of
694 CaMKIV is cAMP response element binding protein (CREB) (Redmond et al., 2002). In normal
695 mice, a high percentage of adult-born GCs express phospho-CREB, the active phosphorylated
696 form of CREB (Nakagawa et al., 2002). Retroviral expression of dominant-negative isoforms of
697 phospho-CREB in newly generated GCs reduced dendritic growth and altered the orientation of
698 dendrites (Jagasia et al., 2009). Conversely, upregulating phospho-CREB in adult-born GCs by a
699 pharmacological approach increased dendritic length and branching (Fujioka et al., 2004).
700 Similarly, incubation of primary hippocampal cultures with cAMP agonists increased the
701 expression of phospho-CREB as well as dendritic length and branching (Fujioka et al., 2004).
702 The expression of phospho-CREB in newly-generated GCs begins around 5 days after the cells
703 become postmitotic and lasts up to about 21 days. The temporal pattern of phospho-CREB
704 expression coincides with the time during which GABA exerts a depolarizing effect on these
705 cells, indicating that GABA-mediated depolarization may play a key role in activation of CREB
706 (Jagasia et al., 2009). One study found that knockdown of NKCC1 in newborn GCs reduced
707 levels of phospho-CREB, indicating a critical role for GABA-mediated depolarization in
708 phosphorylation of CREB at early stages of GC maturation (Jagasia et al., 2009).
709 Brain-Derived Neurotrophic Factor (BDNF) is a key downstream target of CREB. The
710 expression of phospho-CREB in immature adult-born GCs is correlated with maximal expression
711 of BDNF (Bender et al., 2001). Increased glutamatergic neurotransmission increases BDNF
712 levels, while increased GABAergic inhibition decreases BDNF levels (Zafra et al., 1991).
713 Hippocampal slice cultures treated with BDNF showed increased MAP-2 expression and

increased dendritic growth (Marty et al., 1996). Moreover, transplant-derived GABAergic synapses onto adult-born GCs might counteract Hebbian plasticity at excitatory synapses from the entorhinal cortex, as these synapses are also modulated by BDNF (Asztely et al., 2000). Given these prior observations, decreased BDNF release may be responsible for reduced dendritic growth that we observed in adult-born GCs receiving dense inputs from the MGE transplants.

Summary and conclusions

Our results add to a growing body of literature showing that transplantation of MGE-derived GABAergic interneuron progenitors into the mature brain alters host brain neural circuitry. Here, we provide novel findings showing that putative synaptic input from transplants of GABAergic interneuron progenitors was associated with reduced growth of adult-born granule cell dendrites The transplanted interneurons formed putative inhibitory synapses with both proximal and distal dendritic branches, and an overall shortening of dendritic branches was found in adult-born GCs innervated by the transplants in naïve mice. In epileptic mice however, the effect was limited to distal dendrites.

References

Alexander A, Maroso M, Soltesz I (2016) Organization and control of epileptic circuits in temporal lobe epilepsy. Progress in Brain Research 226:127-154.

Althaus AL, Sagher O, Parent JM, Murphy GG (2015) Intrinsic neurophysiological properties of hilar ectopic and normotopic dentate granule cells in human temporal lobe epilepsy and a rat model. Journal of Neurophysiology 113:1184-1194.

Arisi GM, Garcia-Cairasco N (2007) Doublecortin-positive newly born granule cells of hippocampus have abnormal apical dendritic morphology in the pilocarpine model of temporal lobe epilepsy. Brain Research 1165:126-134.

741 Asztely F, Kokaia M, Olofsdotter K, Ortegren U, Lindvall O (2000) Afferent-specific
742 modulation of short-term synaptic plasticity by neurotrophins in dentate gyrus. The
743 European Journal of Neuroscience 12:662-669.
744 Baraban SC, Southwell DG, Estrada RC, Jones DL, Sebe JY, Alfaro-Cervello C, Garcia-
745 Verdugo JM, Rubenstein JL, Alvarez-Buylla A (2009) Reduction of seizures by
746 transplantation of cortical GABAergic interneuron precursors into kv1.1 mutant mice.
747 Proceedings of the National Academy of Sciences of the United States of America
748 106:15472-15477.
749 Bausch SB, McNamara JO (2000) Synaptic connections from multiple subfields contribute to
750 granule cell hyperexcitability in hippocampal slice cultures. Journal of Neurophysiology
751 84:2918-2932.
752 Beck H, Blumcke I, Kral T, Clusmann H, Schramm J, Wiestler OD, Heinemann U, Elger CE
753 (1996) Properties of a delayed rectifier potassium current in dentate granule cells isolated
754 from the hippocampus of patients with chronic temporal lobe epilepsy. Epilepsia 37:892-
755 901.
756 Ben-Ari Y, Khalilov I, Kahle KT, Cherubini E (2012) The GABA excitatory/inhibitory shift in
757 brain maturation and neurological disorders. The Neuroscientist 18:467-486.
758 Bender RA, Lauterborn JC, Gall CM, Cariaga W, Baram TZ (2001) Enhanced CREB
759 phosphorylation in immature dentate gyrus granule cells precedes neurotrophin
760 expression and indicates a specific role of creb in granule cell differentiation. The
761 European Journal of Neuroscience 13:679-686.
762 Borodinsky LN, O'Leary D, Neale JH, Vicini S, Coso OA, Fiszman ML (2003) GABA-induced
763 neurite outgrowth of cerebellar granule cells is mediated by gaba(a) receptor activation,
764 calcium influx and CAMKII and Erk1/2 pathways. Journal of Neurochemistry 84:1411-
765 1420.
766 Buckmaster PS (2012) Mossy fiber sprouting in the dentate gyrus. In: Jasper's Basic Mechanisms
767 of the Epilepsies (th, Noebels JL, Avoli M, Rogawski MA, Olsen RW, Delgado-Escueta
768 AV, eds). Bethesda (MD).
769 Buckmaster PS, Zhang GF, Yamawaki R (2002) Axon sprouting in a model of temporal lobe
770 epilepsy creates a predominantly excitatory feedback circuit. The Journal of
771 Neuroscience 22:6650-6658.
772 Buckmaster PS, Abrams E, Wen X (2017) Seizure frequency correlates with loss of dentate
773 gyrus gabaergic neurons in a mouse model of temporal lobe epilepsy. The Journal of
774 Comparative Neurology 525:2592-2610.
775 Cameron MC, Zhan RZ, Nadler JV (2011) Morphologic integration of hilar ectopic granule cells
776 into dentate gyrus circuitry in the pilocarpine model of temporal lobe epilepsy. The
777 Journal of Comparative Neurology 519:2175-2192.
778 Chiu CQ, Lur G, Morse TM, Carnevale NT, Ellis-Davies GC, Higley MJ (2013)
779 Compartmentalization of GABAergic inhibition by dendritic spines. Science 340:759-
780 762.
781 Cho KO, Lybrand ZR, Ito N, Brulet R, Tafacory F, Zhang L, Good L, Ure K, Kernie SG,
782 Birnbaum SG, Scharfman HE, Eisch AJ, Hsieh J (2015) Aberrant hippocampal
783 neurogenesis contributes to epilepsy and associated cognitive decline. Nature
784 Communications 6:6606.
785 Chohan MO, Moore H (2016) Interneuron progenitor transplantation to treat CNS dysfunction.
786 Frontiers in Neural Circuits 10:64.

787 Cossart R, Dinocourt C, Hirsch JC, Merchan-Perez A, De Felipe J, Ben-Ari Y, Esclapez M,
788 Bernard C (2001) Dendritic but not somatic GABAergic inhibition is decreased in
789 experimental epilepsy. Nature Neuroscience 4:52-62.
790 Cunningham M, Cho JH, Leung A, Savvidis G, Ahn S, Moon M, Lee PK, Han JJ, Azimi N, Kim
791 KS, Bolshakov VY, Chung S (2014) hPSC-derived maturing GABAergic interneurons
792 ameliorate seizures and abnormal behavior in epileptic mice. Cell Stem Cell 15:559-573.
793 Dengler CG, Yue C, Takano H, Coulter DA (2017) Massively augmented hippocampal dentate
794 granule cell activation accompanies epilepsy development. Scientific Reports 7:42090.
795 Du X, Zhang H, Parent JM (2017) Rabies tracing of birthdated dentate granule cells in rat
796 temporal lobe epilepsy. Annals of Neurology 81:790-803.
797 Eid T, Thomas MJ, Spencer DD, Runden-Pran E, Lai JC, Malthankar GV, Kim JH, Danbolt NC,
798 Ottersen OP, de Lanerolle NC (2004) Loss of glutamine synthetase in the human
799 epileptogenic hippocampus: Possible mechanism for raised extracellular glutamate in
800 mesial temporal lobe epilepsy. Lancet 363:28-37.
801 Fujioka T, Fujioka A, Duman RS (2004) Activation of cAMP signaling facilitates the
802 morphological maturation of newborn neurons in adult hippocampus. The Journal of
803 Neuroscience 24:319-328.
804 Ge S, Goh EL, Sailor KA, Kitabatake Y, Ming GL, Song H (2006) GABA regulates synaptic
805 integration of newly generated neurons in the adult brain. Nature 439:589-593.
806 Ghosh A, Greenberg ME (1995) Distinct roles for bfgf and nt-3 in the regulation of cortical
807 neurogenesis. Neuron 15:89-103.
808 Goldberg EM, Coulter DA (2013) Mechanisms of epileptogenesis: A convergence on neural
809 circuit dysfunction. Nature Reviews Neuroscience 14:337-349.
810 Hattiangady B, Shetty AK (2010) Decreased neuronal differentiation of newly generated cells
811 underlies reduced hippocampal neurogenesis in chronic temporal lobe epilepsy.
812 Hippocampus 20:97-112.
813 Hattiangady B, Rao MS, Shetty AK (2004) Chronic temporal lobe epilepsy is associated with
814 severely declined dentate neurogenesis in the adult hippocampus. Neurobiology of
815 Disease 17:473-490.
816 Henderson KW, Gupta J, Tagliatela S, Litvina E, Zheng X, Van Zandt MA, Woods N, Grund E,
817 Lin D, Royston S, Yanagawa Y, Aaron GB, Naegele JR (2014) Long-term seizure
818 suppression and optogenetic analyses of synaptic connectivity in epileptic mice with
819 hippocampal grafts of GABAergic interneurons. The Journal of Neuroscience 34:13492-
820 13504.
821 Hester MS, Danzer SC (2013) Accumulation of abnormal adult-generated hippocampal granule
822 cells predicts seizure frequency and severity. The Journal of Neuroscience 33:8926-8936.
823 Holmes MM, Galea LA, Mistlberger RE, Kempermann G (2004) Adult hippocampal
824 neurogenesis and voluntary running activity: Circadian and dose-dependent effects.
825 Journal of Neuroscience Research 76:216-222.
826 Hosford BE, Liska JP, Danzer SC (2016) Ablation of newly generated hippocampal granule cells
827 has disease-modifying effects in epilepsy. The Journal of Neuroscience 36:11013-11023.
828 Hosford BE, Rowley S, Liska JP, Danzer SC (2017) Ablation of peri-insult generated granule
829 cells after epilepsy onset halts disease progression. Scientific Reports 7:18015.
830 Hsieh JY, Baraban SC (2017) Medial ganglionic eminence progenitors transplanted into
831 hippocampus integrate in a functional and subtype-appropriate manner. eNeuro 4.

Hunt RF, Girskis KM, Rubenstein JL, Alvarez-Buylla A, Baraban SC (2013) GABA progenitors grafted into the adult epileptic brain control seizures and abnormal behavior. Nature Neuroscience 16:692-697.

Jagasia R, Steib K, Englberger E, Herold S, Faus-Kessler T, Saxe M, Gage FH, Song H, Lie DC (2009) GABA-cAMP response element-binding protein signaling regulates maturation and survival of newly generated neurons in the adult hippocampus. The Journal of Neuroscience 29:7966-7977.

Jaiswal MK, Keros S, Zhao M, Inan M, Schwartz TH, Anderson SA, Homanics GE, Goldstein PA (2015) Reduction in focal ictal activity following transplantation of mge interneurons requires expression of the $GABA_A$ receptor alpha4 subunit. Frontiers in Cellular Neuroscience 9:127.

Jessberger S, Romer B, Babu H, Kempermann G (2005) Seizures induce proliferation and dispersion of doublecortin-positive hippocampal progenitor cells. Experimental Neurology 196:342-351.

Jessberger S, Zhao C, Toni N, Clemenson GD, Jr., Li Y, Gage FH (2007) Seizure-associated, aberrant neurogenesis in adult rats characterized with retrovirus-mediated cell labeling. The Journal of Neuroscience 27:9400-9407.

Jiang M, Lee CL, Smith KL, Swann JW (1998) Spine loss and other persistent alterations of hippocampal pyramidal cell dendrites in a model of early-onset epilepsy. The Journal of Neuroscience 18:8356-8368.

LaSarge CL, Santos VR, Danzer SC (2015) Pten deletion from adult-generated dentate granule cells disrupts granule cell mossy fiber axon structure. Neurobiology of Disease 75:142-150.

LaSarge CL, Pun RY, Muntifering MB, Danzer SC (2016) Disrupted hippocampal network physiology following pten deletion from newborn dentate granule cells. Neurobiology of Disease 96:105-114.

Lee H, Yun S, Kim IS, Lee IS, Shin JE, Park SC, Kim WJ, Park KI (2014) Human fetal brain-derived neural stem/progenitor cells grafted into the adult epileptic brain restrain seizures in rat models of temporal lobe epilepsy. PloS One 9:e104092.

Lee JP et al. (2007) Stem cells act through multiple mechanisms to benefit mice with neurodegenerative metabolic disease. Nature Medicine 13:439-447.

Long L, Xiao B, Feng L, Yi F, Li G, Li S, Mutasem MA, Chen S, Bi F, Li Y (2011) Selective loss and axonal sprouting of GABAergic interneurons in the sclerotic hippocampus induced by licl-pilocarpine. The International Journal of Neuroscience 121:69-85.

Luikart BW, Perederiy JV, Westbrook GL (2012) Dentate gyrus neurogenesis, integration and micrornas. Behavioural Brain Research 227:348-355.

Luikart BW, Schnell E, Washburn EK, Bensen AL, Tovar KR, Westbrook GL (2011) Pten knockdown in vivo increases excitatory drive onto dentate granule cells. The Journal of Neuroscience 31:4345-4354.

Marty S, Carroll P, Cellerino A, Castren E, Staiger V, Thoenen H, Lindholm D (1996) Brain-derived neurotrophic factor promotes the differentiation of various hippocampal nonpyramidal neurons, including cajal-retzius cells, in organotypic slice cultures. The Journal of Neuroscience 16:675-687.

Muller CJ, Groticke I, Hoffmann K, Schughart K, Loscher W (2009) Differences in sensitivity to the convulsant pilocarpine in substrains and sublines of C57bl/6 mice. Genes, Brain, and Behavior 8:481-492.

878 Murphy BL, Pun RY, Yin H, Faulkner CR, Loepke AW, Danzer SC (2011) Heterogeneous
879 integration of adult-generated granule cells into the epileptic brain. The Journal of
880 Neuroscience 31:105-117.
881 Nakagawa S, Kim JE, Lee R, Chen J, Fujioka T, Malberg J, Tsuji S, Duman RS (2002)
882 Localization of phosphorylated cAMP response element-binding protein in immature
883 neurons of adult hippocampus. The Journal of Neuroscience 22:9868-9876.
884 Nishimura M, Owens J, Swann JW (2008) Effects of chronic network hyperexcitability on the
885 growth of hippocampal dendrites. Neurobiology of Disease 29:267-277.
886 Nishimura M, Casanova JR, Swann JW (2017) The impact of electrographic seizures on
887 developing hippocampal dendrites is calcineurin dependent. eNeuro 4.
888 Okazaki MM, Evenson DA, Nadler JV (1995) Hippocampal mossy fiber sprouting and synapse
889 formation after status epilepticus in rats: Visualization after retrograde transport of
890 biocytin. The Journal of Comparative Neurology 352:515-534.
891 Parent JM, Elliott RC, Pleasure SJ, Barbaro NM, Lowenstein DH (2006) Aberrant seizure-
892 induced neurogenesis in experimental temporal lobe epilepsy. Annals of Neurology
893 59:81-91.
894 Parent JM, Yu TW, Leibowitz RT, Geschwind DH, Sloviter RS, Lowenstein DH (1997) Dentate
895 granule cell neurogenesis is increased by seizures and contributes to aberrant network
896 reorganization in the adult rat hippocampus. The Journal of Neuroscience 17:3727-3738.
897 Park KI, Teng YD, Snyder EY (2002) The injured brain interacts reciprocally with neural stem
898 cells supported by scaffolds to reconstitute lost tissue. Nature Biotechnology 20:1111-
899 1117.
900 Patel LS, Wenzel HJ, Schwartzkroin PA (2004) Physiological and morphological
901 characterization of dentate granule cells in the p35 knock-out mouse hippocampus:
902 Evidence for an epileptic circuit. The Journal of Neuroscience 24:9005-9014.
903 Peng Z, Zhang N, Wei W, Huang CS, Cetina Y, Otis TS, Houser CR (2013) A reorganized
904 gabaergic circuit in a model of epilepsy: Evidence from optogenetic labeling and
905 stimulation of somatostatin interneurons. The Journal of Neuroscience 33:14392-14405.
906 Pun RY, Rolle IJ, Lasarge CL, Hosford BE, Rosen JM, Uhl JD, Schmeltzer SN, Faulkner C,
907 Bronson SL, Murphy BL, Richards DA, Holland KD, Danzer SC (2012) Excessive
908 activation of mtor in postnatally generated granule cells is sufficient to cause epilepsy.
909 Neuron 75:1022-1034.
910 Redmond L, Kashani AH, Ghosh A (2002) Calcium regulation of dendritic growth via cam
911 kinase iv and creb-mediated transcription. Neuron 34:999-1010.
912 Santos VR, Pun RYK, Arafa SR, LaSarge CL, Rowley S, Khademi S, Bouley T, Holland KD,
913 Garcia-Cairasco N, Danzer SC (2017) Pten deletion increases hippocampal granule cell
914 excitability in male and female mice. Neurobiology of Disease 108:339-351.
915 Scharfman HE (2005) Brain-derived neurotrophic factor and epilepsy--a missing link? Epilepsy
916 Currents 5:83-88.
917 Scharfman HE, Goodman JH, Sollas AL (2000) Granule-like neurons at the hilar/ca3 border
918 after status epilepticus and their synchrony with area ca3 pyramidal cells: Functional
919 implications of seizure-induced neurogenesis. The Journal of Neuroscience 20:6144-
920 6158.
921 Scharfman HE, Sollas AL, Berger RE, Goodman JH (2003a) Electrophysiological evidence of
922 monosynaptic excitatory transmission between granule cells after seizure-induced mossy
923 fiber sprouting. Journal of Neurophysiology 90:2536-2547.

924 Scharfman HE, Sollas AE, Berger RE, Goodman JH, Pierce JP (2003b) Perforant path activation
925 of ectopic granule cells that are born after pilocarpine-induced seizures. Neuroscience
926 121:1017-1029.
927 Schmidt-Hieber C, Jonas P, Bischofberger J (2004) Enhanced synaptic plasticity in newly
928 generated granule cells of the adult hippocampus. Nature 429:184-187.
929 Shetty AK, Upadhya D (2016) GABA-ergic cell therapy for epilepsy: Advances, limitations and
930 challenges. Neuroscience and Biobehavioral Reviews 62:35-47.
931 Shibley H, Smith BN (2002) Pilocarpine-induced status epilepticus results in mossy fiber
932 sprouting and spontaneous seizures in c57bl/6 and cd-1 mice. Epilepsy Research 49:109-
933 120.
934 Southwell DG, Froemke RC, Alvarez-Buylla A, Stryker MP, Gandhi SP (2010) Cortical
935 plasticity induced by inhibitory neuron transplantation. Science 327:1145-1148.
936 Spatazza J, Mancia Leon WR, Alvarez-Buylla A (2017) Transplantation of gabaergic
937 interneurons for cell-based therapy. Progress in Brain Research 231:57-85.
938 Thind KK, Ribak CE, Buckmaster PS (2008) Synaptic input to dentate granule cell basal
939 dendrites in a rat model of temporal lobe epilepsy. The Journal of Comparative
940 Neurology 509:190-202.
941 Vogt D, Wu PR, Sorrells SF, Arnold C, Alvarez-Buylla A, Rubenstein JL (2015) Viral-mediated
942 labeling and transplantation of medial ganglionic eminence (mge) cells for in vivo
943 studies. Journal of Visualized Experiments : JoVE.
944 von Campe G, Spencer DD, de Lanerolle NC (1997) Morphology of dentate granule cells in the
945 human epileptogenic hippocampus. Hippocampus 7:472-488.
946 Walter C, Murphy BL, Pun RY, Spieles-Engemann AL, Danzer SC (2007) Pilocarpine-induced
947 seizures cause selective time-dependent changes to adult-generated hippocampal dentate
948 granule cells. The Journal of Neuroscience 27:7541-7552.
949 Wilson MD, Sethi S, Lein PJ, Keil KP (2017) Valid statistical approaches for analyzing sholl
950 data: Mixed effects versus simple linear models. Journal of Neuroscience Methods
951 279:33-43.
952 Woods NI, Vaaga CE, Chatzi C, Adelson JD, Collie MF, Perederiy JV, Tovar KR, Westbrook
953 GL (2018) Preferential targeting of lateral entorhinal inputs onto newly integrated
954 granule cells. The Journal of Neuroscience 38:5843-5853.
955 Xu Q, Cobos I, De La Cruz E, Rubenstein JL, Anderson SA (2004) Origins of cortical
956 interneuron subtypes. The Journal of Neuroscience 24:2612-2622.
957 Yu W, Krook-Magnuson E (2017) Targeting newly generated granule cells: A double-edged
958 sword. Epilepsy Currents 17:121-123.
959 Zafra F, Castren E, Thoenen H, Lindholm D (1991) Interplay between glutamate and gamma-
960 aminobutyric acid transmitter systems in the physiological regulation of brain-derived
961 neurotrophic factor and nerve growth factor synthesis in hippocampal neurons.
962 Proceedings of the National Academy of Sciences of the United States of America
963 88:10037-10041.
964 Zhang W, Yamawaki R, Wen X, Uhl J, Diaz J, Prince DA, Buckmaster PS (2009) Surviving
965 hilar somatostatin interneurons enlarge, sprout axons, and form new synapses with
966 granule cells in a mouse model of temporal lobe epilepsy. The Journal of Neuroscience
967 29:14247-14256.

968 Zipancic I, Calcagnotto ME, Piquer-Gil M, Mello LE, Alvarez-Dolado M (2010) Transplant of
969 GABAergic precursors restores hippocampal inhibitory function in a mouse model of
970 seizure susceptibility. Cell Transplantation 19:549-564.
971

972 **Figure Legends**

973 **Figure 1. Experimental timeline for RV-labeling of adult-born granule cells in naïve and**
974 **SE mice**. **A**, Different groups of mice studied and the experimental timelines for each group
975 including: timing of retroviral injections (RV), day of transplantation of embryonic day 13.5
976 MGE progenitors (TX), day of optogenetic and patch-clamp electrophysiological experiments,
977 and 3D neuronal reconstructions and Sholl analyses. **B**, RV-expression (mCherry, red) in a
978 dentate GC showing labeling of dendritic arbor and axon. **C**, Patterns of RV-labeled GCs in an
979 adult naïve mouse. **D**-**G**, Patterns of RV-labeling in adult-born GCs in TLE mice following
980 retroviral injections at 1-, 2-, 6-, or 12-weeks post-SE. Scale equals 20 μm in B, Scales equal 200
981 μm in C-G.
982

983 **Figure 2. Functional inhibition from transplanted ChR2-expressing MGE-derived**
984 **GABAergic interneurons onto a mature adult-born GC labeled with RV 1-week after SE.**
985 Transplanted interneurons were optogenetically stimulated while performing patch-clamp
986 recordings from adult-born, RV-labeled GCs in hippocampal slices. **A**, Low-magnification
987 image of the DG in an SE mouse that received injections of RV at 1-week post-SE and a
988 transplant at 2-weeks post-SE. Boxed area shows RV-labeled GCs (red), and white arrow
989 indicates the RV-labeled GC that was further characterized by patch-clamp electrophysiology,
990 optogenetic stimulation, and biocytin staining (blue). Various interneuron subtypes comprising
991 the transplant are shown in extended data figure 2-1. **B**, Higher magnification view of the boxed
992 region in A; the electrophysiologically-characterized and biocytin-filled GC is indicated by a

white arrow in the group of adult-born GCs (red) **C**, Magnified view of the same group of RV-labeled adult-born GCs (red) showing the presence of dense plexus of MGE-derived ChR2-EYFP-expressing GABAergic axons (green). Note that due to photobleaching, the density of axons appears to be reduced around the cell bodies. **D**, Same biocytin-filled GC (white) surrounded by transplanted MGE-derived ChR2-EYFP-expressing GABAergic interneurons and their axonal arbors (green). **E**, High magnification single optical slice showing dendritic segment of the biocytin-filled GC (white) and transplant-derived putative synaptic boutons (green). Arrows indicate sites of putative synaptic contacts by the transplanted interneurons onto this GC. **F**, A partial reconstruction of the same biocytin-filled GC (red). The yellow dots indicate the locations of putative inhibitory synaptic contacts from the transplants. **G**, Electrophysiological recording of this GC showing optogenetically-induced IPSCs, following blue-light stimulation of the ChR2-expressing transplanted interneurons (vertical blue bars indicate blue light pulses of 5 msec duration, and 200 msec interpulse interval). Scale bar: A, 200 µm. B, C, 50 µm. D, 20 µm. E, 2 µm.

Figure 2-1. Extended data: Transplanted MGE-derived ChR2-EYFP-expressing GABAergic interneuron progenitors differentiate into multiple subtypes of GABAergic interneurons. A-D, Examples of transplanted interneurons that co-expressed EYFP and PV (n= 3 mice; 207 cells) in ML and GCL of the dentate gyrus. A magnified view of a representative cell is shown in **D. E-H,** MGE-derived GABAergic interneurons expressing SOM (n= 3 mice; 232 cells) were localized primarily near the injection site in the DG. A magnified view of a representative SOM^+ cell is shown in H. **I-L,** Examples of transplanted $nNos^+$ MGE-derived interneurons (n= 3 mice; 73 cells). These cells were located in the ML and hilus of the dentate

gyrus; a magnified image of a representative $nNos^+$ cell is shown in L. **M-O,** Some MGE-derived cells in the grafts expressed CR (n= 3 mice; 52 cells) and were localized in the ML and hilus. The strong band of CR^+ staining in N is from CR^+ axons. **P,** A magnified view of the CR^+ cell shown in M-O. **Q,** Quantification of the proportions of each cell type were as follows: 37.3% PV^+, 33.8%, SOM^+, 12.4% $nNos^+$ and 7.9% CR^+. **R-T,** Example of an MGE-derived transplanted interneuron that was characterized by patch-clamp electrophysiology and stained with biocytin. **R,** Boxed region shows a low-power view of this large interneuron within a transplant. **S,** The inset from R shows a higher-magnification image of the transplanted interneuron. **T,** An IMARIS-based reconstruction of the transplanted interneuron from R-T. Arrows; VGAT-ChR2-EYFP interneurons co-expressing indicated neurochemical markers. Scale bars equal A-C, E-G, I-K, M-O, S, 50 µm; D, H, L, P, 20 µm; R, 200 µm. Abbreviations: ML, molecular layer; GCL, granule cell layer.

Figure 3. Amplitudes of optogenetically-activated inhibitory postsynaptic currents in granule cells strongly correlate with number of synaptic inputs from transplanted GABAergic interneurons. A-C Optogenetically-induced synaptic currents were measured in adult-born GCs generated 2, 6- or 12-weeks post-SE, by whole-cell patch clamping and subsequently filled with biocytin (white). **A'-C',** Merged images of filled GCs showing mCherry expression (red), biocytin-fill (blue) and transplant arborization (green) in these slices. **A''-C''.** Synaptic innervation of adult-born GCs shown in A-C demonstrated by optogenetic activation of transplanted interneurons. **D, E,** GCs located outside of the region innervated by the transplanted GABAergic interneurons did not show optogenetically induced currents. **F, Summary graph from all recorded GCs (both RV-labeled and non-labeled) showing strong correlation**

1039 **between** the density of transplant-derived boutons and the peak amplitude of light-induced
1040 inhibitory currents. Adult-born GCs with confirmed RV-labeling are indicated by colored
1041 triangle-shaped symbols. The blue triangles are GCs labeled 1-week post SE; the green triangles
1042 are GCs labeled 2-weeks post-SE; the red triangles are GCs labeled 12-weeks post-SE. The gray
1043 circles are GCs with unknown birthdates.
1044
1045 **Figure 4. Transplanted GABAergic interneurons innervate adult-born granule cells in**
1046 **naïve mice. A**, Low magnification image showing RV-labeled adult-born GCs (red) surrounded
1047 by a transplant of ChR2-eYFP expressing interneurons (green) in the DG of a naïve mouse.
1048 Boxed region in A, biocytin-filled (blue) and retrovirally labeled (red) adult-born GC that was
1049 characterized by whole-cell patch clamp electrophysiology. **B**, Magnified view of the boxed
1050 region in A, the same biocytin-filled GC is shown to co-express mCherry. **C**, Biocytin-filled GC
1051 (pseudo-colored white for enhanced visibility) surrounded by neuropil from transplanted MGE-
1052 derived GABAergic interneurons (green). **D**, Electrophysiological recording from this GC
1053 showing postsynaptic IPSCs induced by exciting the ChR2-expressing interneurons in this
1054 transplant. Vertical blue bars indicated blue light pulses delivered to the slice. **E**, Sholl analyses
1055 of the dendritic arbor of this GC provide quantification of dendritic crossings every 10 µm
1056 interval from the cell's soma. **F**, IMARIS 3-D reconstruction of this GC showing distribution of
1057 putative transplant-derived synapses (yellow dots). Scale bars equal A, 100 µm, B, 50 µm, C, 20
1058 µm.
1059
1060 **Figure 5. Transplanted GABAergic interneurons innervate adult-born GCs born 6 weeks**
1061 **after SE. A**, Low magnification image showing adult-born GCs (red) surrounded by ChR2-

eYFP expressing transplants (green) in a mouse that had SE. Boxed region shows the biocytin-filled (blue) adult-born GC that was recorded in this slice using whole-cell patch clamping. **B**, Magnified view of the boxed region, showing co-labeling with biocytin and mCherry. **C**, View of the biocytin-filled GC (white) and surrounding axons from transplanted MGE-derived GABAergic interneurons (green). **D**, Electrophysiological recording from this GC showed a moderate response to optogenetic activation of the ChR2-expressing transplanted interneurons and a distinct IPSC can be seen in response to the first light-pulse. **E**, Sholl analysis graph of the number of dendritic intersections. **F**, Complete neuronal reconstruction of this GC and the sites of putative transplant-derived synapses (yellow dots). Scale bars: A, 100 µm. B, 50 µm. C, 20 µm.

Figure 6. Adult-born granule cells innervated by transplanted GABAergic interneurons develop significantly shorter distal dendrites. A, Bar graph of total dendritic lengths in transplant-innervated and non-innervated adult-born GCs in different experimental groups.. All neurons were confirmed to be adult-born and retrovirally-labeled by immunostaining for mCherry expression. Data for non-innervated GCs is represented by purple bars and innervated GCs are shown in green bars. GCs with high levels of putative synaptic input from the transplanted GABAergic interneurons had significantly shorter dendrites than non-innervated adult-born GCs. Neuronal reconstructions of the GCs in different experimental groups are shown in extended data figures 6-1 to 6-5. **B,** Schematic of the Sholl analysis paradigm for analysis of dendritic branching based on number of dendritic branches intersecting concentric spheres spaced at 10 µm intervals from the soma. C-H, Sholl analyses of dendritic arbors comparing transplant-innervated adult-born GCs (green lines) vs. non-innervated GCs (purple lines).

Shading represents standard error of the means (SEM). C, In the naïve mice, innervated GCs showed reduced dendritic branching both proximally and distally, compared with non-innervated GCs. D, Grouped Sholl data showing significantly reduced dendritic arbors in innervated, adult-born GCs compared to non-innervated adult-born GCs. While the innervated GCs formed similar patterns of proximal branching, they had significantly fewer distal branches, compared to non-innervated adult-born GCs. Significant differences found for radii at 150 microns from the soma (p value 0.03) and all radii between 170-290 microns from the soma ($P < 0.01$). **E-H,** Sholl data broken down by the birthdate post-SE of adult-born GCs. Graphs indicate that innervated adult-born GCs had significantly fewer distal dendrites, compared to non-innervated adult-born GCs. **E,** Innervated GCs born 1-week post-SE had significantly fewer intersections at radii between 200-270 microns from the soma, compared to non-innervated GCs ($P < 0.05$). **F,** Innervated GCs born 2 weeks post-SE had significantly reduced dendritic branching at radii 200-250 microns compared to the non-innervated GCs ($P < 0.05$). **G,** Innervated GCs born 6 weeks post-SE had significantly fewer dendritic branches at radii 150-270 microns compared to non-innervated GCs ($P < 0.05$). **H,** Innervated GCs born 12 weeks after SE showed trend toward reduced branching compared to non-innervated GCs, but this trend did not reach significance. Asterisks indicate statistically significant differences between groups.

Figure 6-1. Extended data: Neuronal reconstructions of RV-labeled GCs from naïve mice. Representative neuronal reconstructions of the dendritic arbors of adult-born GCs with confirmed expression of RV-expression of mCherry. Mature neuronal arbors of innervated and non-innervated GCs are shown ~ 8 weeks after RV-labeling and 9 weeks after MGE transplantation. Scale equals 100 μm.

Figure 6-2. Extended data: Neuronal reconstructions of GCs labeled with RV 1-week after SE. Comparisons of mature dentate GCs that were born 1-week after SE in mice that received transplants at 2-weeks after SE. Innervated and non-innervated GCs shown 8 weeks after MGE transplantation (10 weeks post-SE). Scale equals 100 μm.

Figure 6-3. Extended data: Neuronal reconstructions of mature GCs labeled with RV 2-weeks after SE. Comparisons of mature dentate GCs that were born 2-weeks after SE in mice that received transplants at 6 weeks after SE. Innervated and non-innervated GCs are shown 8 weeks after MGE transplantation (14 weeks post-SE). Scale equals 100 μm.

Figure 6-4. Extended data: Neuronal reconstructions of 8-week-old GCs labeled with RV 6-weeks after SE. Comparisons of mature dentate GC dendritic arbors in cells that were born 6-weeks after SE in mice that received MGE transplants 2 weeks after SE. Innervated and non-innervated GCs are shown ~8-weeks after transplantation (14 weeks post-SE). Scale equals 100 μm.

Figure 6-5. Extended data: Neuronal reconstructions of 8-10-week-old GCs labelled with RV 12-weeks after SE. Representative neuronal reconstructions from populations of innervated and non-innervated GCs that were born 12 weeks post-SE in mice that received transplants at 2 weeks after SE. Innervated and non-innervated GCs are shown approximately ~ 18 weeks after transplantation (20 weeks post-SE). Scale equals 100 μm.

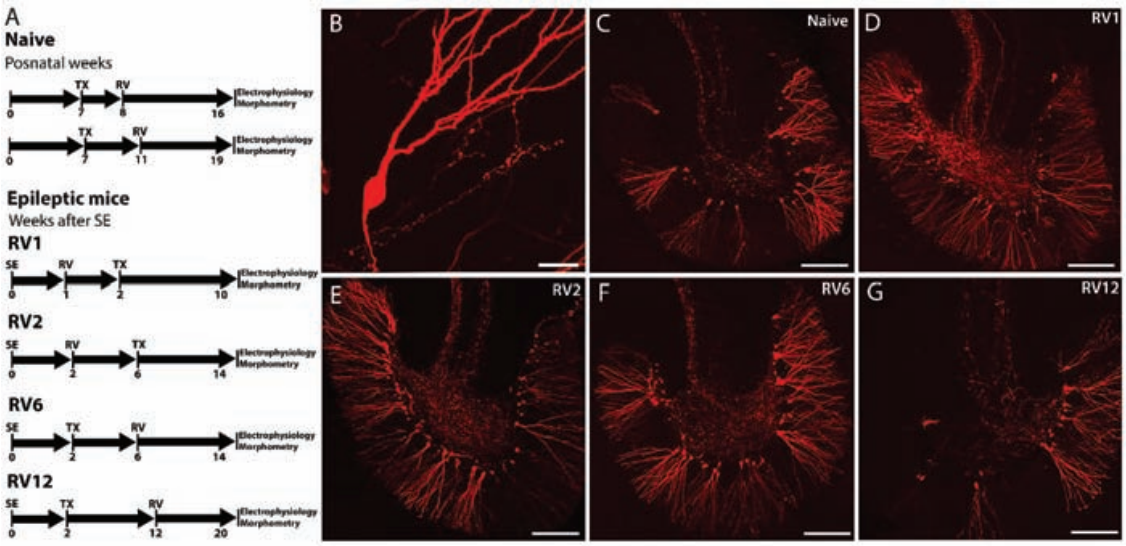

Figure 1

1147

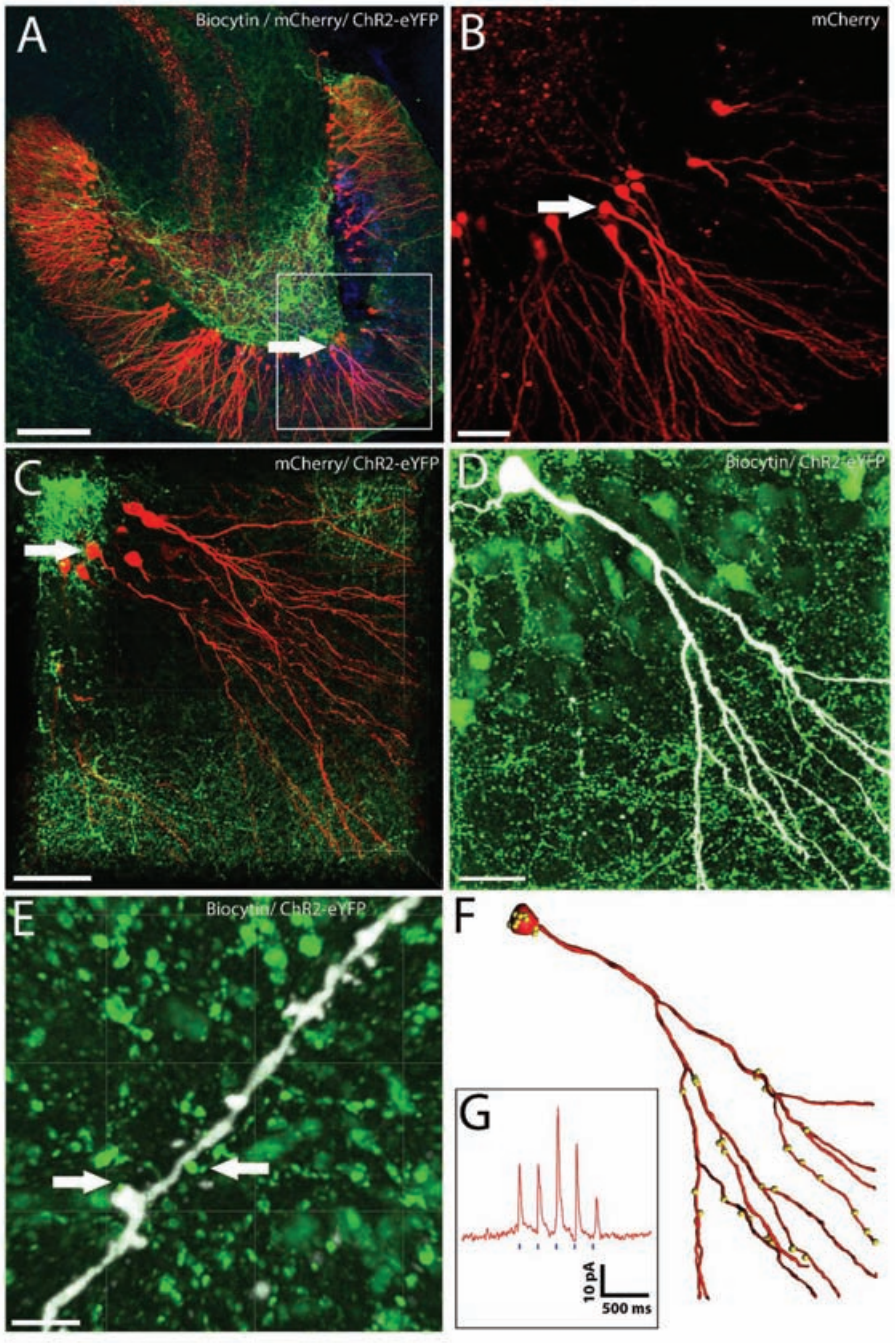

1148

1149 **Figure 2**

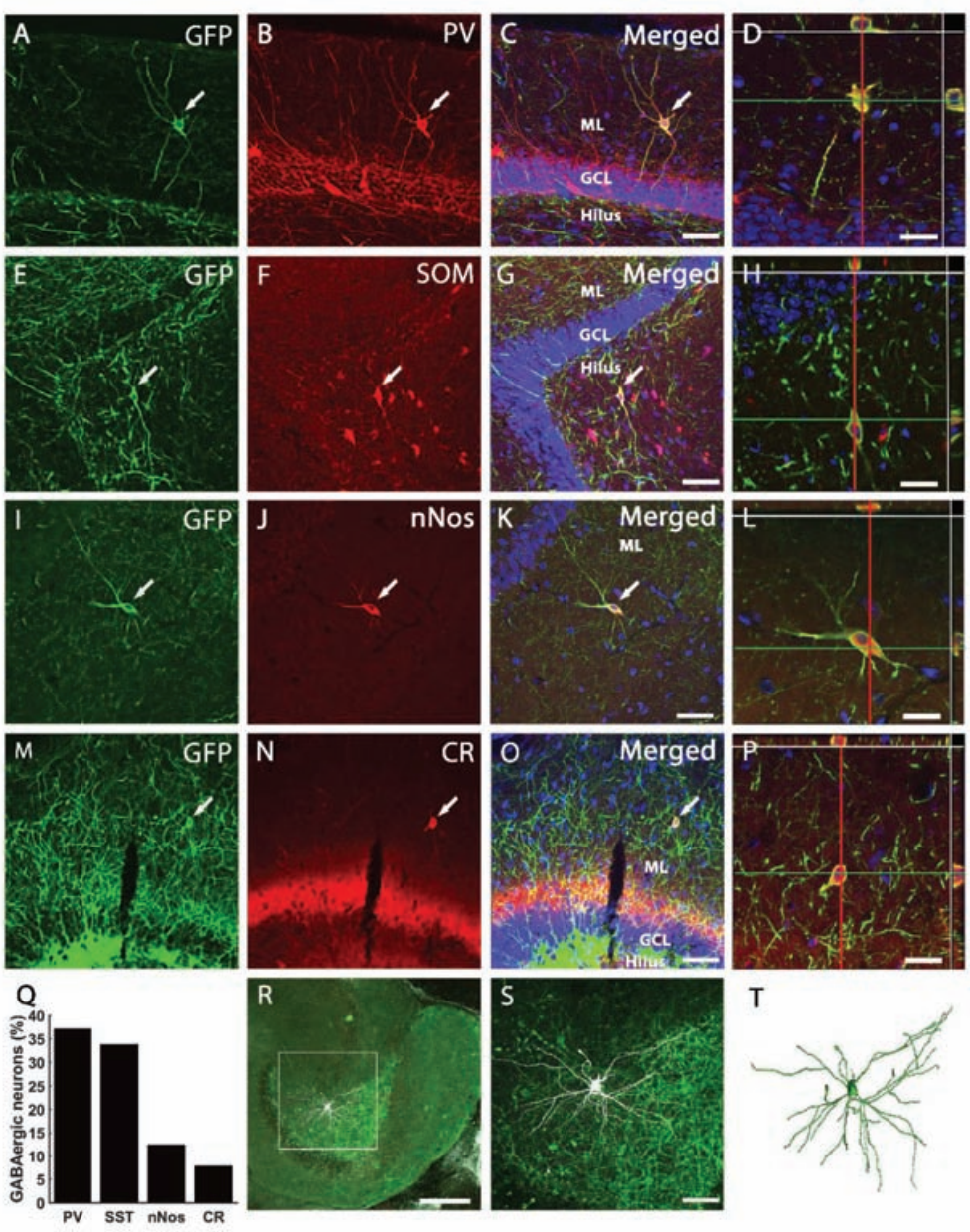

1150

1151 **Figure 2-1**

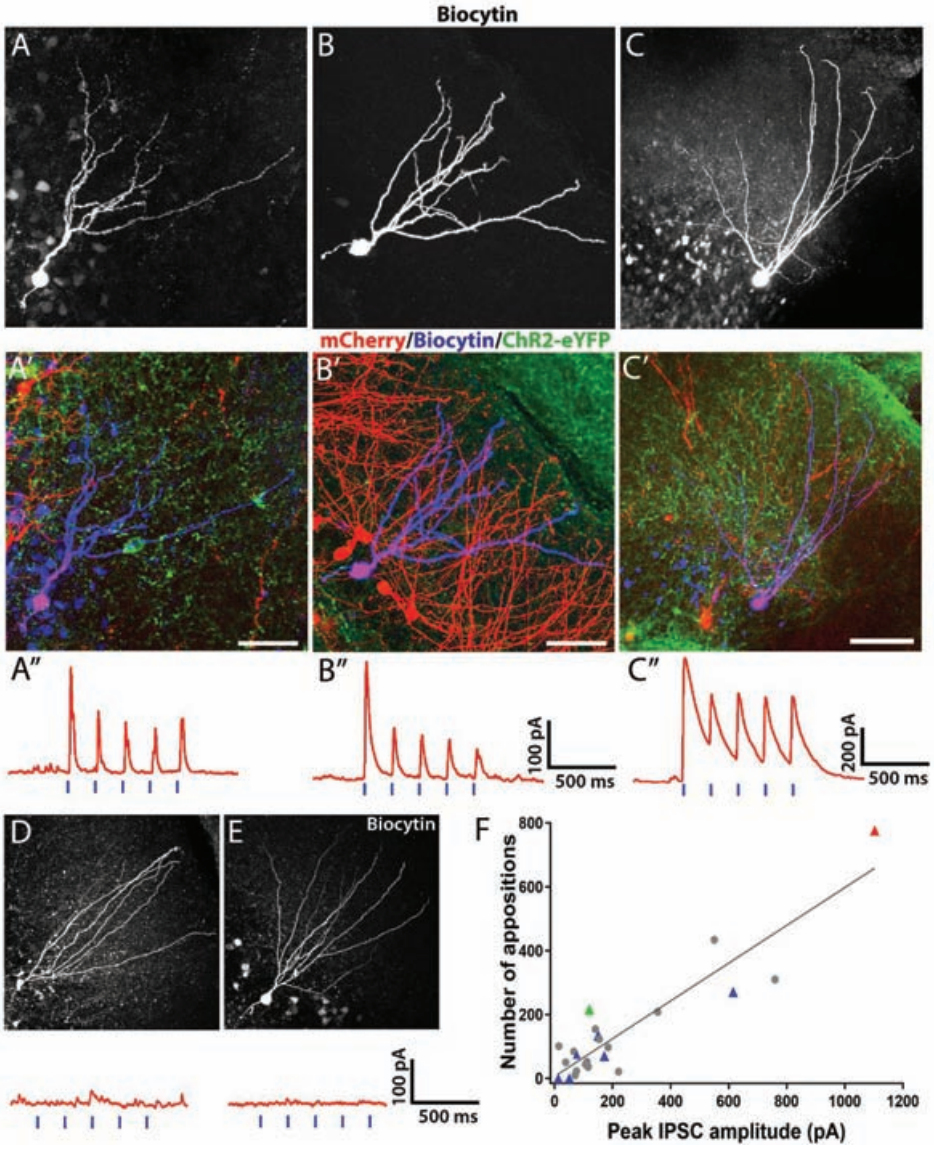

1152

1153

1154

1155 **Figure 3**

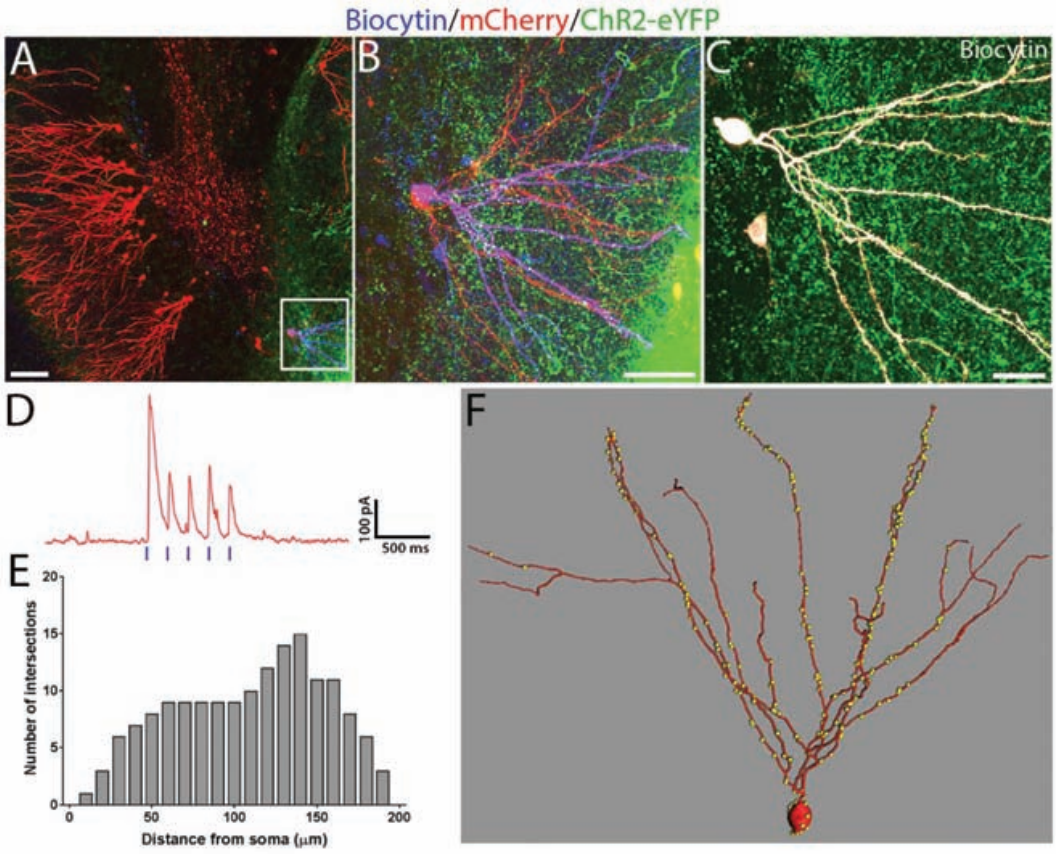

Figure 4

1166

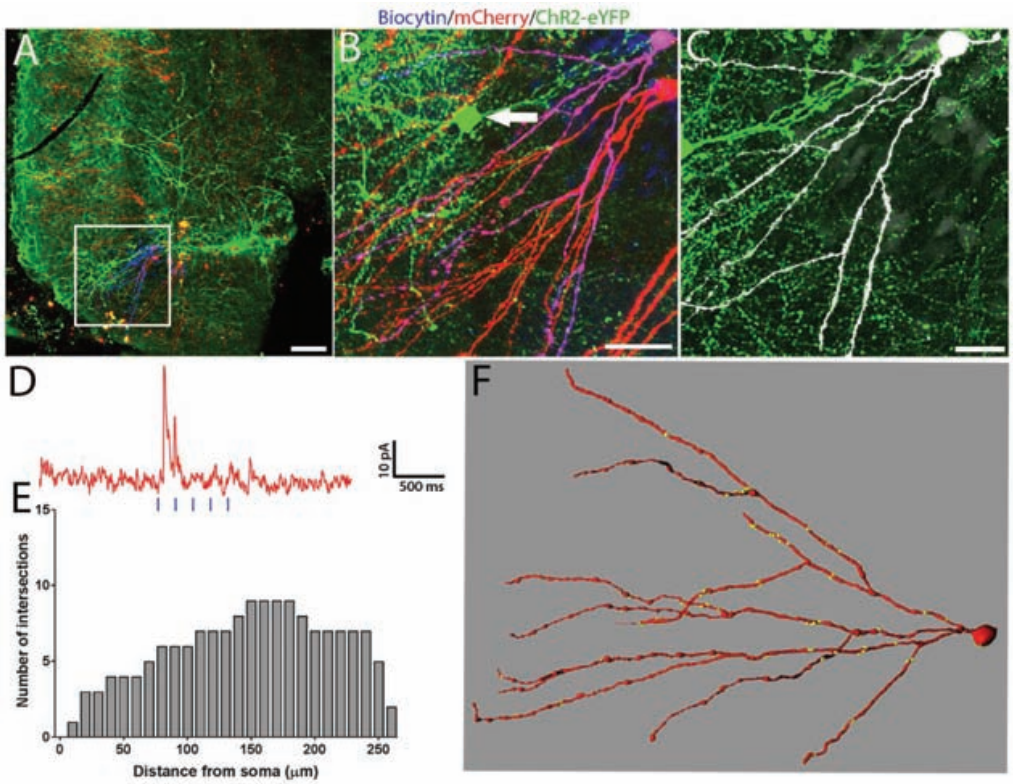

1167

1168

1169 **Figure 5**

1170

1171

1172

1173

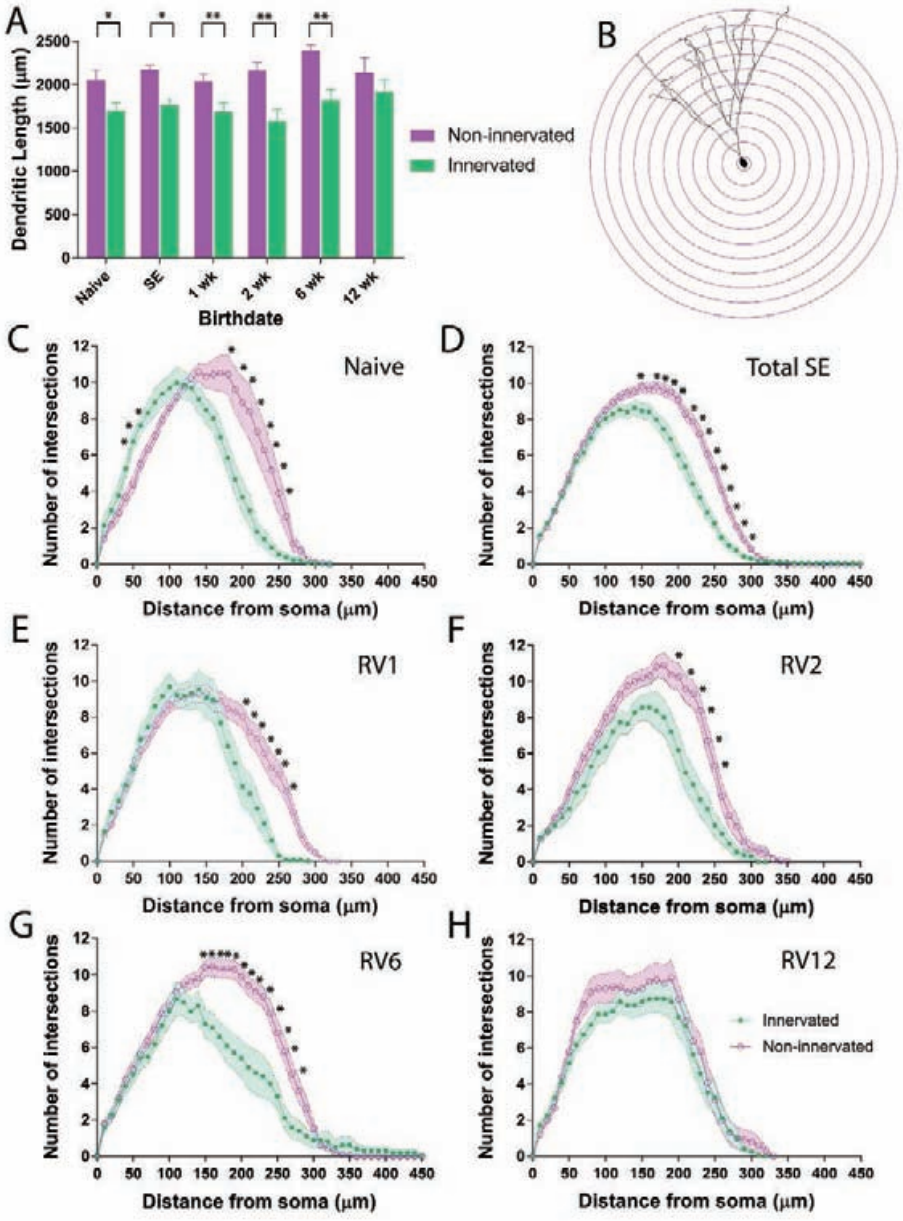

1194 **Figure 6**

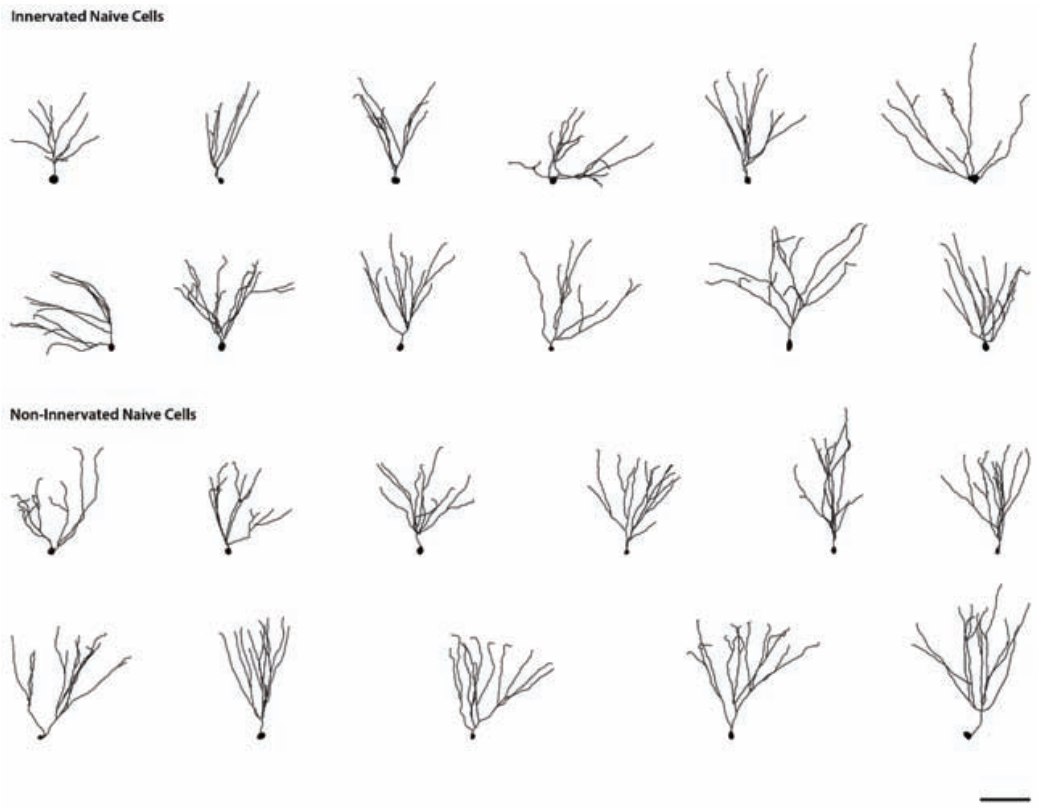

Figure 6-1

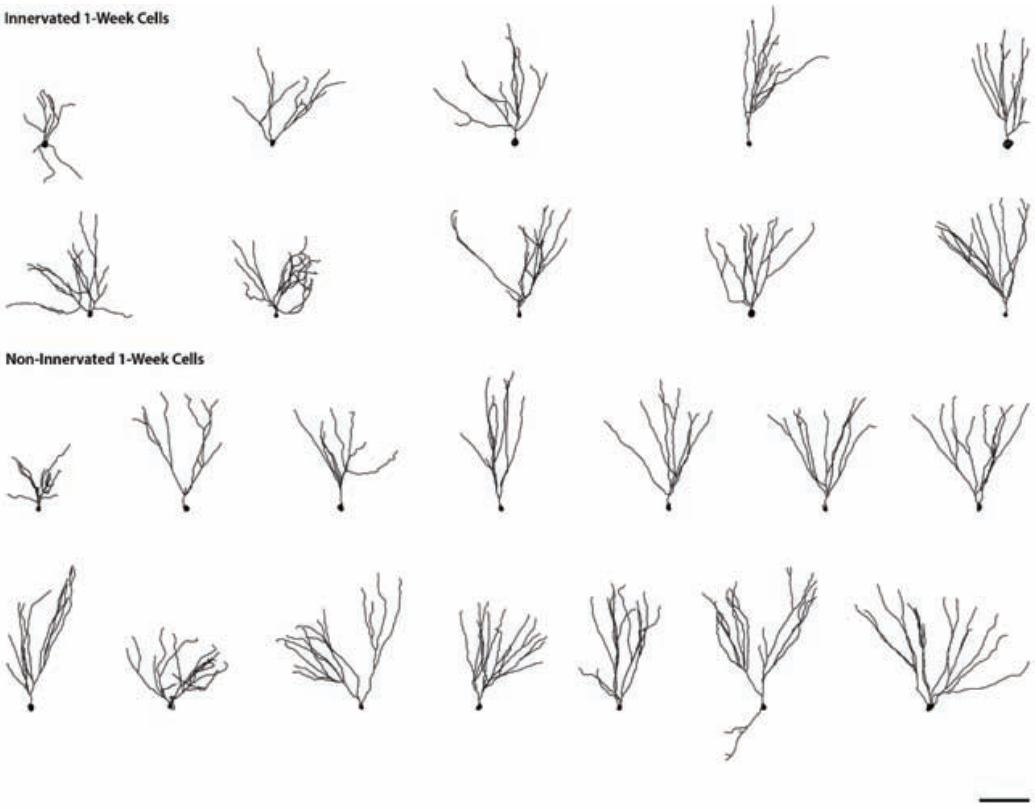

Figure 6-2

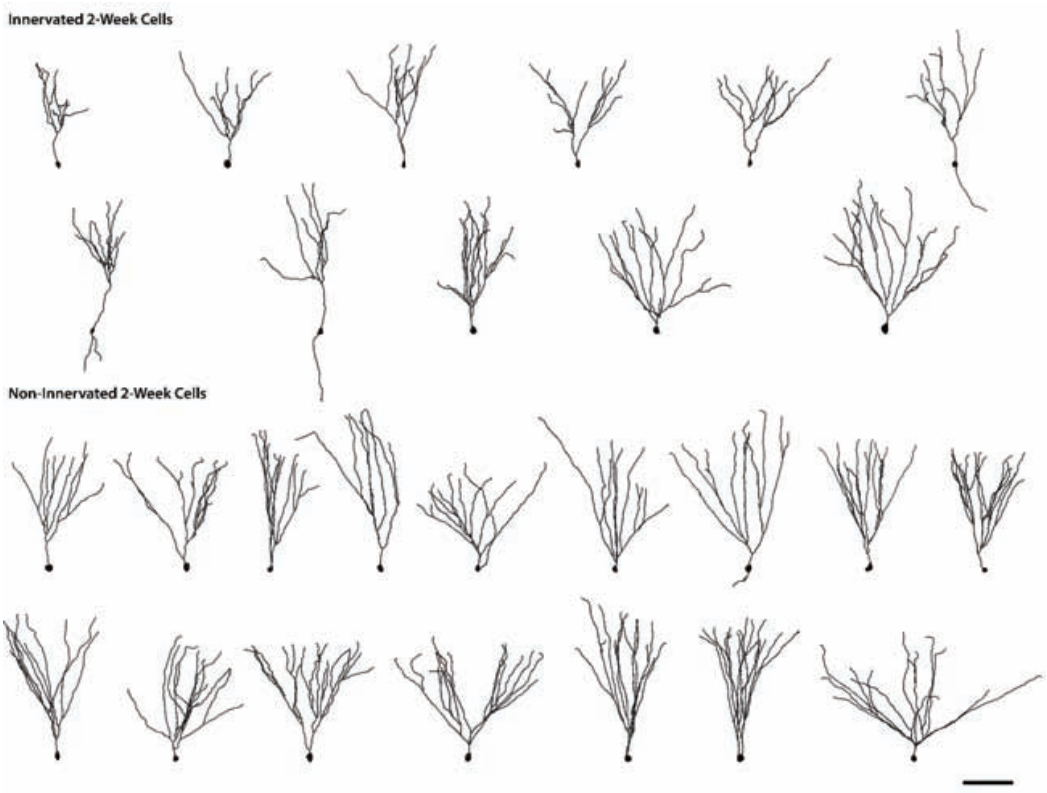

Figure 6-3

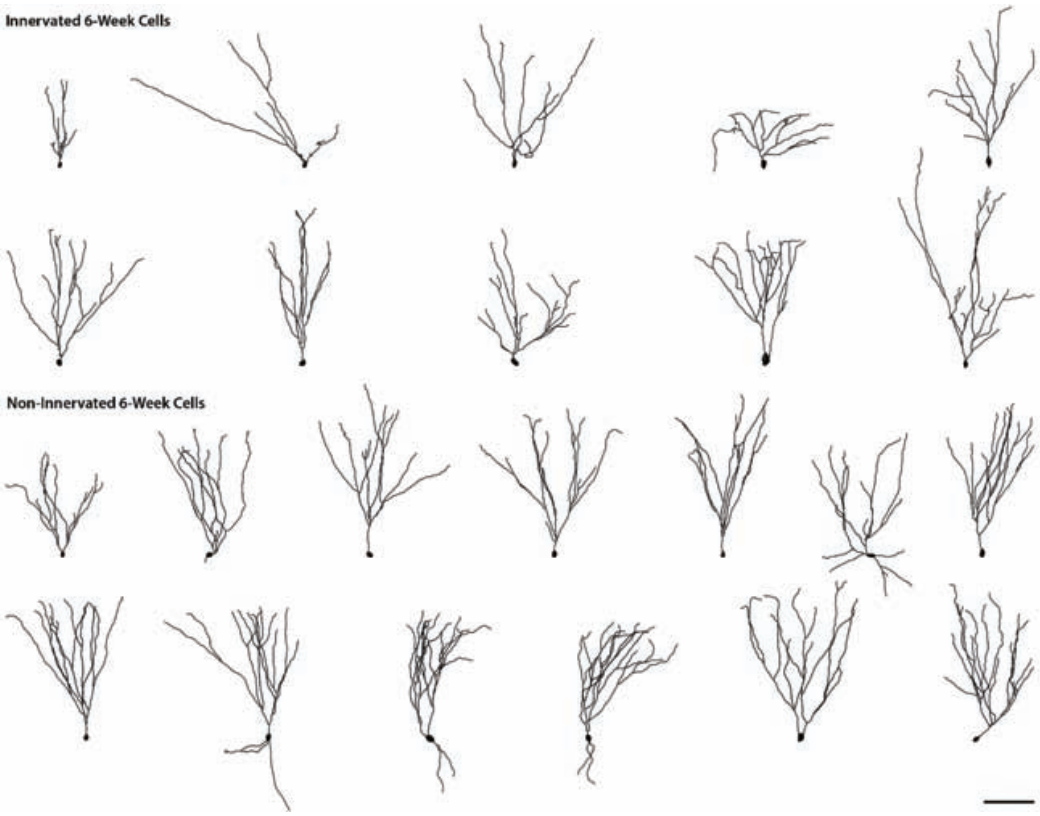

Figure 6-4

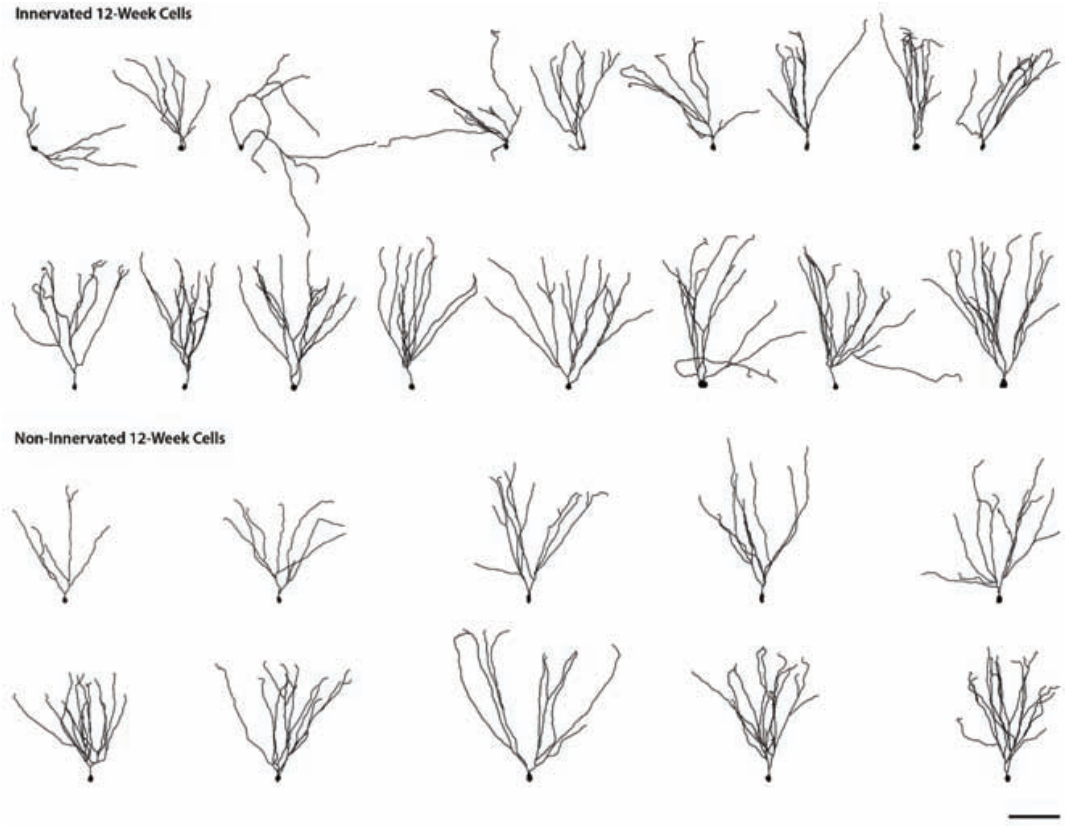

Figure 6-5

1247

1248

Table 1. Summary table for number of GCs recorded				
	Number of mice	**Number of recorded retrovirally-labelled GCs**	**Number of GCs that responded to light-stimulation**	**Number of responsive GCs that were morphologically recovered following electrophysiology and confirmed to be RV labelled**
1-week RV	6	23	10	6
2 weeks RV	5	15	8	2
6 weeks RV	5	13	8	5
12 weeks RV	2	4	4	1

1249

1250

Table 2. Key Resources		
REAGENT or RESOURCE	**SOURCE**	**IDENTIFIER**
Antibodies		
Anti-GFP (Green Fluorescent Protein) (Chicken antibodies, IgY fraction)	Aves	GFP-1020
Rabbit mCherry	Invitrogen	PA5-34974
Streptavidin, Alexa Fluor® 647 conjugate	Invitrogen	S32357
Alexa Fluor® 488 goat anti-chicken (H+L)	Life Technologies	A11039
Alexa Fluor® 568 goat anti-rabbit IgG (H+L)	Life Technologies	P36971
Plasmids		
pRubi	Luikart Lab (Dartmouth)	
redRubi	Luikart Lab (Dartmouth)	
Chemicals, Media		
ProLong™ Diamond Antifade Mountant with DAPI	Invitrogen	P36971
Iscove's Modification of DMEM	Corning	10-016-CV
L-Glutamine, 100x, Liquid	Corning	25-005-CI
MEM Nonessential Amino Acids	Corning	25-025-CI
Penicillin-Streptomycin Solution, 100X	Corning	30-002-CI
PEG 6000, Molecular Biology Grade	Millipore Sigma	528877
L-15 Medium (Leibovitz) with L-glutamine	Sigma-Aldrich	SLBR4210V
Defined Trypsin Inhibitor (1X)	Gibco	R-007-100
2.5% Trypsin (10X)	Gibco	15090-046
Mouse EGF	Cell Signaling	5331SF
Fibroblast Growth Factor-basic Human	Cell Signaling	F0291
B-27 Supplement	Gibco	17504-044
Caspase Inhibitor Z-VAD-FMK 20mM	Promega	G7231
Commercial Kits		
NucleoBond Xtra Maxi DNA, RNA and protein purification kit	Macherey-Nagel	740414.10
Experimental Models: Cell Lines		
293 GP	Luikart Lab (Dartmouth)	
293 R	Luikart Lab (Dartmouth)	
Experimental Models: Mice		
C57BL/NHsd	Envigo	
B6.Cg-Tg(Slc32a1-COP4*H134R/EYFP)8Gfng/J (VGAT-ChR2-EYFP line 8)	The Jackson Laboratory	014548
Software: IMARIS	Bitplane	

1251

Table 3: Total dendritic lengths for different groups of mice					
Quantitative measurement	**GCs from naïve mice**	**GCs labelled at 1-week post-SE**	**GCs labelled at 2 weeks post-SE**	**GCs labelled at 6 weeks post-SE**	**GCs labelled at 12 weeks post-SE**
Corrected *p* value **(using mixed effects model)**	0.0235	0.0129	0.0027	0.0010	0.3211
Mean (µm)	Non-innervated: 2055.6 Innervated: 1700.0	Non-innervated: 2039.9 Innervated: 1690.1	Non-innervated: 2161.6 Innervated: 1577.7	Non-innervated: 2390.0 Innervated: 1825.3	Non-innervated: 2143.3 Innervated: 1917.0
Std. Dev.	Non-innervated: 493.9 Innervated: 331.8	Non-innervated: 452.5 Innervated: 365.9	Non-innervated: 371.6 Innervated: 466.0	Non-innervated: 316.7 Innervated: 380.1	Non-innervated: 529.1 Innervated: 606.1
N (GCs)	Non-innervated: 18 Innervated: 13	Non-innervated: 29 Innervated: 13	Non-innervated: 16 Innervated: 11	Non-innervated: 20 Innervated: 10	Non-innervated: 10 Innervated: 17
N (total GCs)	31	42	27	30	27

1257

Table 4: Statistical comparisons of Sholl data and significance values for all retrovirally-labeled, adult-born granule cells
(statistically significant *p* values equal to or less than 0.05 are shown in red)

Radius	Naive	SE	1-week RV	2 weeks RV	6 weeks RV	12 weeks RV
10	0.1727	0.4666	0.8371	0.6229	0.7329	0.5425
20	0.2448	0.4000	0.4370	0.8628	0.9167	0.7634
30	0.2568	0.8828	0.8884	0.3471	0.8933	0.7634
40	0.0634	0.5937	0.9445	0.5976	0.7329	0.7840
50	0.0321	0.3749	0.9445	0.2050	0.7795	0.7634
60	0.0321	0.5723	0.8349	0.3316	0.8529	0.5425
70	0.0321	0.2545	0.7540	0.1376	0.2966	0.5425
80	0.0526	0.4145	0.4370	0.2771	0.4499	0.5425
90	0.0979	0.4885	0.5077	0.3397	0.6101	0.5968
100	0.1765	0.3608	0.4370	0.1376	0.7921	0.6550
110	0.3591	0.2357	0.9445	0.2050	0.7795	0.7328
120	0.9248	0.1969	0.9445	0.1294	0.3682	0.7634
130	0.6053	0.0556	0.9445	0.0489	0.0894	0.7634
140	0.1727	0.1535	0.9445	0.1009	0.1800	0.7634
150	0.1213	0.0314	0.9445	0.1158	0.0039	0.7634
160	0.0953	0.0551	0.9445	0.1158	0.0054	0.7634
170	0.0513	0.0059	0.5871	0.1009	0.0028	0.7634
180	0.0321	0.0026	0.2395	0.0733	0.0028	0.7634
190	0.0321	0.0005	0.0742	0.0660	0.0028	0.7634
200	0.0321	0.0005	0.0174	0.0263	0.0028	0.7634
210	0.0364	0.0005	0.0368	0.0100	0.0028	0.9482
220	0.0321	0.0005	0.0196	0.0090	0.0035	0.7968
230	0.0377	0.0005	0.0196	0.0090	0.0029	0.7634
240	0.0498	0.0005	0.0174	0.0380	0.0056	0.8077
250	0.0526	0.0005	0.0084	0.0270	0.0140	0.9482
260	0.0953	0.0005	0.0084	0.1294	0.0095	0.9482
270	0.1765	0.0005	0.0174	0.1974	0.0307	0.9482
280	0.2245	0.0044	0.0742	0.1974	0.0894	1.000
290	0.3591	0.0071		0.2900	0.1810	0.7634
300	0.7866	0.0559		0.4536	0.4722	0.7634
310		0.2357			0.6300	0.5968
320		0.4962			0.6179	
330		0.9539			0.5304	
340		0.4414			0.3078	
350		0.3117			0.2551	
360		0.2284				
370		0.1969				
380		0.1969				
390		0.1969				
400		0.1969				
410		0.3117				
420		0.3117				
430		0.3117				
440		0.3117				

1258